Molecular Cell

Article

The TRESLIN-MTBP complex couples completion of DNA replication with S/G2 transition

Graphical abstract

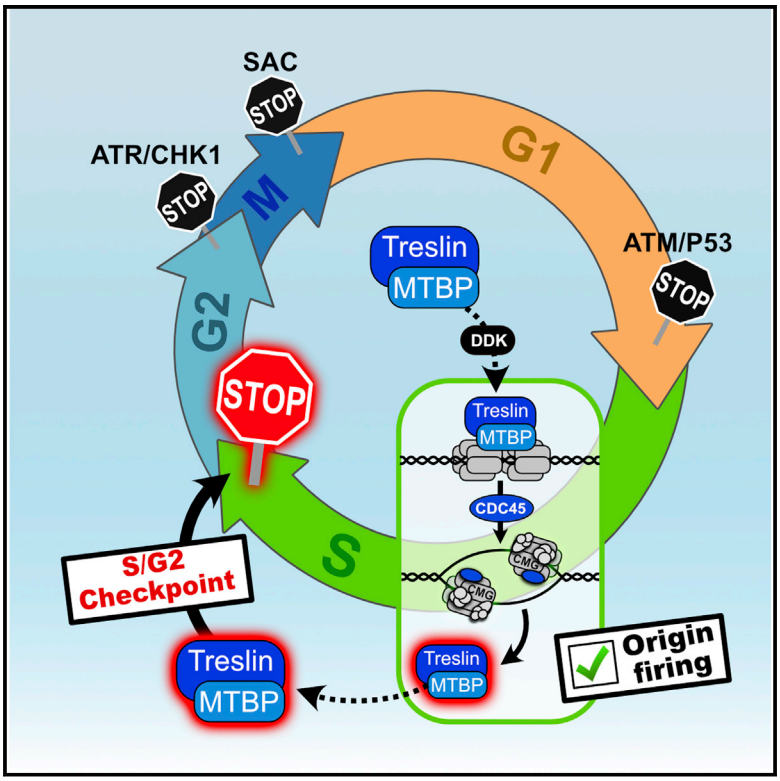

Highlights

- TRESLIN-MTBP checks the firing of replication origins to manage S-phase progression
- Activation of CMGs by CDC45 releases TRESLIN-MTBP from DNA to monitor origin firing
- Cells lacking TRESLIN-MTBP transition into G2 from the start of DNA replication
- The S/G2 transition is regulated by TRESLIN-MTBP independently of ATR/CHK1 kinases

Authors

Gijs Zonderland, Riccardo Vanzo, Sampath Amitash, ..., Jan Benada, Dominik Boos, Luis Toledo

Correspondence

ltoledo@sund.ku.dk

In brief

Cells need to ensure complete genome duplication before dividing. Zonderland et al. describe that the TRESLIN-MTBP complex monitors origin firing to couple DNA replication and the timely progression from S- to G2-phase. Unlike previously thought, the S/G2 checkpoint is implemented independently of ATR and CHK1 kinases.

Zonderland et al., 2022, Molecular Cell *82*, 3350–3365
September 15, 2022
https://doi.org/10.1016/j.molcel.2022.08.006

CellPress

CellPress
OPEN ACCESS

Molecular Cell

Article

The TRESLIN-MTBP complex couples completion of DNA replication with S/G2 transition

Gijs Zonderland,[1] Riccardo Vanzo,[1] Sampath Amitash,[1] Elena Martín-Doncel,[1] Fabian Coscia,[2,3] Andreas Mund,[3] Mads Lerdrup,[1] Jan Benada,[4] Dominik Boos,[5] and Luis Toledo[1,6,*]

[1]Center for Chromosome Stability, Institute for Cellular and Molecular Medicine, Faculty of Health and Medical Sciences, University of Copenhagen, Copenhagen 2200, Denmark
[2]Max Delbrück Center for Molecular Medicine (MDC), 13092 Berlin, Germany
[3]Novo Nordisk Foundation Center for Protein Research, Faculty of Health and Medical Sciences, University of Copenhagen, Copenhagen 2200, Denmark
[4]Biotech Research & Innovation Centre, Faculty of Health and Medical Sciences, University of Copenhagen, Copenhagen 2200, Denmark
[5]Vertebrate DNA Replication Lab, Centre for Medical Biotechnology, University of Duisburg-Essen, 45141 Essen, Germany
[6]Lead contact
*Correspondence: ltoledo@sund.ku.dk
https://doi.org/10.1016/j.molcel.2022.08.006

SUMMARY

It has been proposed that ATR kinase senses the completion of DNA replication to initiate the S/G2 transition. In contrast to this model, we show here that the TRESLIN-MTBP complex prevents a premature entry into G2 from early S-phase independently of ATR/CHK1 kinases. TRESLIN-MTBP acts transiently at pre-replication complexes (preRCs) to initiate origin firing and is released after the subsequent recruitment of CDC45. This dynamic behavior of TRESLIN-MTBP implements a monitoring system that checks the activation of replication forks and senses the rate of origin firing to prevent the entry into G2. This system detects the decline in the number of origins of replication that naturally occurs in very late S, which is the signature that cells use to determine the completion of DNA replication and permit the S/G2 transition. Our work introduces TRESLIN-MTBP as a key player in cell-cycle control independent of canonical checkpoints.

INTRODUCTION

A key function of the cell cycle is to ensure that the genome is fully replicated before cells commit to chromosome segregation. How cells monitor the progression of DNA replication to prevent a premature entry into mitosis has been a paramount question in the cell-cycle field for decades. Cell-cycle checkpoints in yeast, controlled by Mec1 and Rad53 kinases (in budding yeast), have a key role in preventing premature mitosis (reviewed in Labib and De Piccoli, 2011). In humans, however, this role has been less clear. The human homologs of Mec1 and Rad53, ATR (ataxia telangiectasia and Rad3 related), and CHK1 (checkpoint kinase 1), respectively, have been studied as key responders to replication stress (RS) and DNA damage (reviewed in Zeman and Cimprich, 2014), but they are also active under normal conditions during S-phase (Brown and Baltimore, 2000; Eykelenboom et al., 2013; Moiseeva et al., 2019; Syljuåsen et al., 2005; Toledo et al., 2013). Cells rely on this ATR/CHK1 activity to limit CDK2 activity and regulate the firing of replication origins throughout S-phase (Daigh et al., 2018; Maya-Mendoza et al., 2007; Moiseeva et al., 2017; Shechter et al., 2004; Syljuåsen et al., 2005; Toledo et al., 2013). This function prevents the pathological accumulation of active forks, which can lead to the exhaustion of dNTPs and replication catastrophe (Toledo et al., 2013). Recently, it was shown that ATR/CHK1 prevent a premature transition into G2 and mitosis by limiting CDK1 activity, delaying the transcription of mitotic factors and the activation of mitotic kinases (Lemmens et al., 2018; Saldivar et al., 2018). Because this intrinsic activity is dependent on the presence of single-stranded DNA (ssDNA) at active replication forks, ATR/CHK1 implement a DNA replication monitoring system which ensures that CDK1 activity is restrained until the genome has been fully duplicated (Saldivar et al., 2018).

However, the ability of ATR/CHK1 to prevent a premature mitotic entry is rather limited and restricted to the latest stages of S-phase (Eykelenboom et al., 2013; Ruiz et al., 2016; Saldivar et al., 2018). Although cells can slip into G2/M prematurely in the absence of ATR/CHK1 activity, most cells remain in S-phase under the same conditions, implying that additional processes linked to DNA replication may regulate the separation between S-phase and G2/M (Lemmens et al., 2018). Interestingly, the product of the *ticcr* gene TRESLIN (homolog of budding yeast Sld3) prevents mitotic entry from S-phase in zebrafish (Sansam et al., 2010). TRESLIN (and its partner MTBP, homolog of yeast Sld7) is critical for origin firing in humans, a process that requires the sequential recruitment of several proteins to pre-

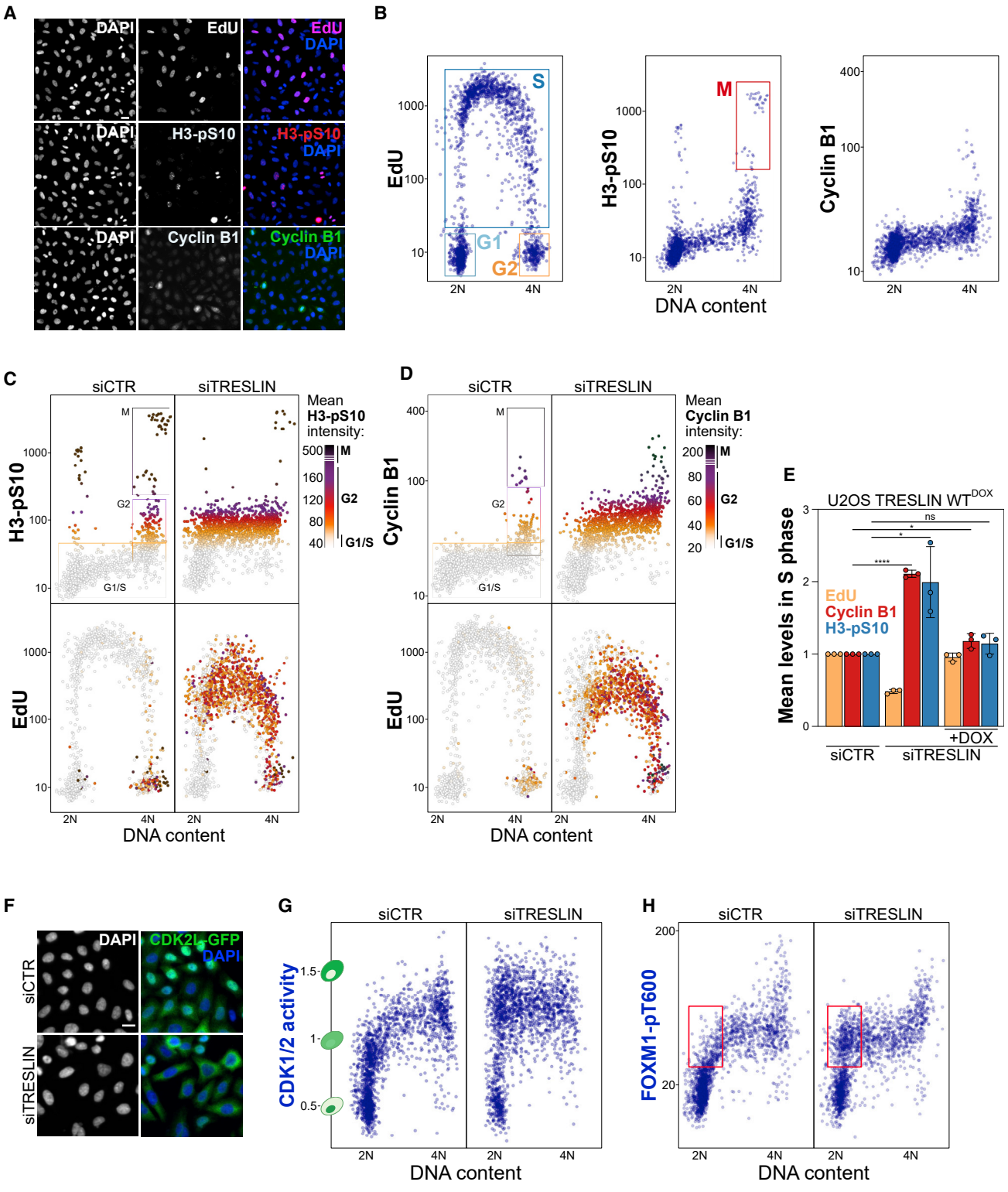

Figure 1. Depletion of TRESLIN causes an uncoupling of DNA replication and cell-cycle status

(A) HeLa cells stained for EdU, H3-pS10, cyclin B1, and DAPI. Scale bar is 20 μm.

(B) QIBC of cells stained as in (A). Boxes highlight different cell-cycle stages.

(legend continued on next page)

replication complexes (preRCs) (Fragkos et al., 2015). TRESLIN binds MCMs phosphorylated by DDK (DBF4/CDC7) and is essential for the recruitment of CDC45. TRESLIN is also phosphorylated by CDK2, which enhances its interaction with TOPBP1 at preRCs (Boos et al., 2011, 2013; Kumagai et al., 2010, 2011; Mueller et al., 2011; Volpi et al., 2021). Independently, RECQL4 is required to load the GINS complex to finalize the formation of the CDC45-MCM2-7-GINS replicative helicase (Muramatsu et al., 2010). How TRESLIN regulates cell cycle progression, and whether this is linked to DNA replication, remains unexplored.

Here, we show that the human TRESLIN-MTBP complex couples the end of DNA replication with the transition into G2. Importantly, this is a function independent of the ATR/CHK1 pathway that relies on TRESLIN activity at preRCs to monitor origin firing during S-phase.

RESULTS

TRESLIN-MTBP couples DNA replication with cell-cycle status

To examine the role of human TRESLIN in cell-cycle progression, we devised a quantitative analysis of the S-G2/M transition in single cells using quantitative image based cytometry (QIBC) (Toledo et al., 2013). We imaged HeLa cells and quantified the levels of DAPI intensity (to determine DNA content), EdU incorporation (to monitor DNA replication), and histone H3 phosphorylation on Serine 10 (H3-pS10, to visualize mitotic entry). With these, we could precisely identify G1, S, G2, and M phases in asynchronously growing cells (Figures 1A and 1B). We also quantified the levels of cyclin B1, whose expression is markedly linked to G2 entry (Figures 1A and 1B). Multicolor QIBC analysis of HeLa cells revealed that both cyclin B1 and H3-pS10 rose slightly from the beginning of S-phase but quickly increased after DNA synthesis had ceased, peaking in early mitosis (Figures 1C and 1D). These data suggest that there is a tight control mechanism that couples the end of DNA replication with the beginning of G2.

Next, we depleted TRESLIN with a siRNA against *ticrr*, which led to a marked decrease in EdU levels and a S-phase arrest, consistent with its role in origin firing (Figure S1A). Surprisingly, both cyclin B1 and H3-pS10 levels were abnormally high throughout S-phase in siTRESLIN cells (Figures 1C and 1D). This phenotype was also seen in U2OS cells and was rescued by re-expressing a siRNA-resistant wild-type TRESLIN (Figures 1E, S1B, and S1C). Similar results were obtained in MCF-7 and hTERT RPE-1 cells (Figure S1D). Knocking down TRESLIN's interaction partner MTBP caused a similar phenotype, rescued by wild-type MTBP (Figure S1E), and partial knockdown of both MTBP and TRESLIN showed strong synergy (Figure S1F). Overall, these results demonstrate that the TRESLIN-MTBP complex prevents a premature progression of the cell cycle.

Since CDK activity is the main driver of the cell cycle, we checked whether TRESLIN depletion was associated with a premature hyper-activation of CDKs. We generated HeLa cells expressing a CDK1/2 activity live reporter (Barr et al., 2016; Gu et al., 2004; Spencer et al., 2013) (Figures 1F and S1G), which was validated using different agents (Figure S1H). QIBC showed that CDK1/2 activity rose quickly in G1 and gradually throughout S until peaking in G2 (Figure 1G). As expected, CDK activity was abnormally high throughout S-phase in siTRESLIN cells (Figure 1G). Validating this, CDK-dependent FOXM1 phosphorylation on T600 raised prematurely in siTRESLIN cells, particularly in the beginning of S-phase (Saldivar et al., 2018) (Figure 1G).

In contrast to zebrafish embryos (Sansam et al., 2010), S-phase human cells depleted of TRESLIN were not in a mitotic state. H3-pS10 levels were much lower than those in metaphase/anaphase (Figures 1B and 1C), and no sign of chromosome condensation or nuclear envelope breakdown (NEB) was found (Figure S1I). To discard that this phenotype was a consequence of abnormalities in previous cell cycles (Spencer et al., 2013), we arrested cells with thymidine from the moment of siRNA transfection. Non-cycling TRESLIN-depleted cells had elevated levels of cyclin B1 similar to their cycling counterparts (Figure S1J). Together, these data suggest that TRESLIN depletion does not cause mitotic entry per se but a widespread uncoupling of DNA replication and cell-cycle progression already from early S-phase.

Cells enter G2 prematurely in the absence of TRESLIN-MTBP

To further understand the effects of TRESLIN depletion on the cell cycle, we analyzed by QIBC the expression of cyclins E1 and A2. As expected, cyclin E1 was highest in G1 and was gradually degraded in S-phase (Figure 2A). Cyclin A2 increased after G1 exit and peaked in G2 (Figure 2B). TRESLIN depletion induced a dramatic change in these expression profiles, causing cyclin E1 to be degraded and cyclin A2 to accumulate already at the beginning of S-phase (Figures 2A and 2B). Interestingly, the levels of all three A2, B1, and E1 cyclin in S-phase after TRESLIN depletion were similar to those normally found in G2 (Figure 2C). Furthermore, the levels and localization of H3-pS10 in siTRESLIN S-phase cells were similar to control G2 cells (Hendzel et al., 1997) (Figure 2D). Accordingly, H3-pS10 was dependent on AURKA, as it normally is during G2 (Roeschert et al., 2021)

(C and D) QIBC of HeLa cells transfected with the indicated siRNAs and stained with the indicated markers 48 h after. 10 μM EdU was added for the last 30 min. Boxes indicate different cell-cycle stages, which are used as reference for color thresholds (see STAR Methods for details). Note that data for siCTR in (C) and (D) were used for the cartoon in (B).

(E) Related to Figures S1B and S1C. Statistics of 3 independent experiments as in Figures S1B and S1C (n = 3 ± SD). Mean intensities in S-phase were obtained from EdU-positive cells scored as in (B). *$p < 0.05$; ****$p < 0.0001$, unpaired t test.

(F) Images of HeLa cells harboring CDK1/2 reporter transfected with the indicated siRNAs (48 h). Scale bar is 20 μm.

(G) QIBC of cells in (F).

(H) QIBC of cells transfected as in (G) stained for FOXM1-pT600 and DAPI. Red box highlights cells in early S-phase.

All QIBC data are representative of ≥3 independent biological replicates.

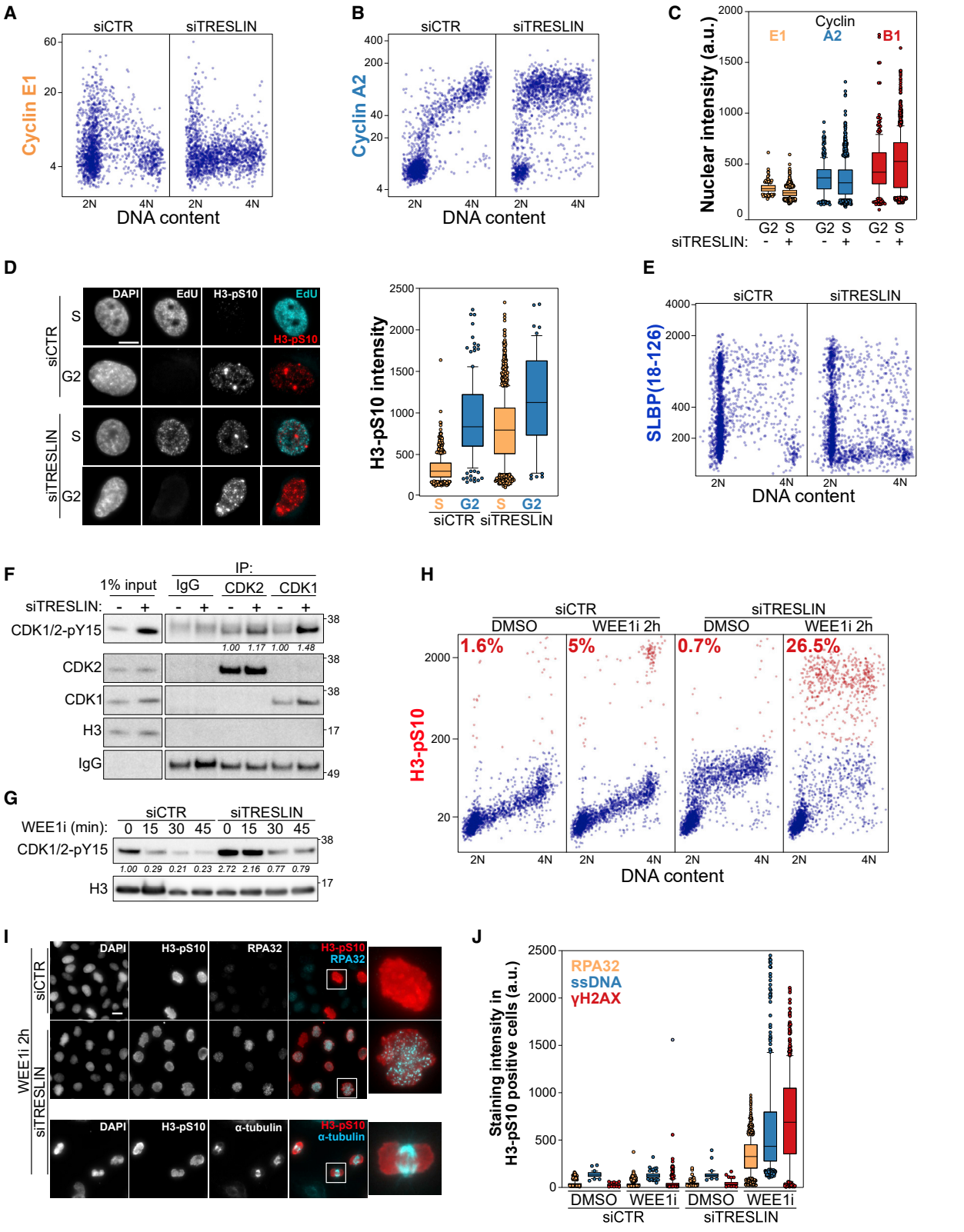

(legend on next page)

(Figure S2A). siTRESLIN also caused the premature degradation of SLBP$^{(18–126)}$, a marker for G2 entry (Bajar et al., 2016; Koseoglu et al., 2008), supporting that these cells enter into a *bona fide* G2 prematurely (Figures 2E and S2B).

Supporting these data, a proteomic analysis confirmed the changes in all three cyclins observed by QIBC (Figure S2C). Additionally, a number of pro-mitotic regulators were upregulated in siTRESLIN cells (Figure S2C). These data indicate that the changes occurring at the proteome level in siTRESLIN cells resemble a late stage of the cell cycle. Changes at the proteome level correlated with those of early transcriptome (particularly for key cell-cycle regulators), as shown by RNA-seq analysis of siTRESLIN HeLa cells (Figure S2D). Although protein levels might deviate due to other post-transcriptional processes, this is in line with the S/G2 transition being mainly triggered by CDK-mediated transcriptional changes and with the elevated FOXM1-pT600 in siTRESLIN cells (Figure 1G) (Laoukili et al., 2005; Sadasivam et al., 2012; Saldivar et al., 2018). Consistently, both CDK activity and cyclin B1 expression observed in these cells were largely dependent on cyclin A2. Interestingly though, FOXM1-pT600 levels in early S-phase were cyclin A2 independent, suggesting other mechanisms leading to the premature activation of CDK1/2 in siTRESLIN cells (Figure S2E).

Despite the indications of high CDK1/2 activity and pro-mitotic cyclins A2 and B1, siTRESLIN cells seemed arrested in a *bona fide* stable G2 state throughout S-phase. This suggested that CDK1 activity could be restrained by inhibitory phosphorylations (i.e., on Y15). Interestingly, immunoprecipitation of CDK1 and CDK2 showed that pY15 levels were particularly higher in CDK1, a result consistent with siTRESLIN cells being in a pre-mitotic arrest (Figure 2F). pY15 could be reversed by treating cells with a WEE1 inhibitor (Figure 2G). Consistently, WEE1 inhibition caused a rapid mitotic entry in S-phase siTRESLIN cells, evidenced by H3-pS10 levels, chromosome condensation, spindle formation, and NEB (Figures 2H, 2I, S2F, and S2G). Mitotic entry was dependent on PLK1 activity (Figure S2G) and caused a widespread accumulation of ssDNA and DNA damage in siTRESLIN cells (Figures 2I and 2J), an indication of massive fork breakage.

TRESLIN and ATR have independent but complementary functions in cell-cycle control

TRESLIN has been shown to promote ATR activation *in vitro* when overexpressed (Hassan et al., 2013). Therefore, it is plausible that TRESLIN acts upstream of ATR, and the cell-cycle disruption observed in siTRESLIN cells is a consequence of impairing ATR/CHK1 signaling. As shown previously (Saldivar et al., 2018), inhibition of ATR or CHK1 led to a premature accumulation of cyclin B1 (Figure 3A). This was restricted to late S-phase, whereas other documented effects of inhibiting these kinases, such as the induction of origin firing and RPA loading, were observed throughout S-phase (Figure 3A) (Daigh et al., 2018; Moiseeva et al., 2019; Toledo et al., 2013). In comparison, TRESLIN depletion led to a rise in cyclin B1 levels already at early S-phase (Figure 3A). Depletion of the known ATR and CHK1 activators (TOPBP1, ETAA1, or CLASPIN) caused no significant changes in cyclin B1 levels or FOXM1-pT600 comparable with siTRESLIN cells (Figures 3B and S3A–S3C). Surprisingly, joint depletion of ETAA1 and TOPBP1 had no effect on cyclin B1 expression, questioning whether ATR is involved physiologically in the S/G2 transition. These results indicate that the effect of impairing TRESLIN or the ATR/CHK1 pathway on the cell cycle are different.

To check whether ATR/CHK1 and TRESLIN act in the same pathway, we analyzed ATR/CHK1 signaling siTRESLIN cells. ATR activation in response to RS was similar to siCTR in response to hydroxyurea (HU) (Figure 3C). Surprisingly, both CHK1-pS296 and γH2AX were elevated in untreated siTRESLIN cells (Figures 3D and 3E), indicating a spontaneous activation of ATR, not due to RS. Consistently, the elevated γH2AX in siTRESLIN cells was ETAA1 dependent (Figure 3E) (Achuthankutty et al., 2019; Haahr et al., 2016; Saldivar et al., 2018). We could not detect spontaneous phosphorylation of S345 or S317 in siTRESLIN cells (although both increased in response to HU in an ATR-dependent manner) (Figures S3D and S3E), which is consistent with ETAA1 having a more specific role in regulating ATR/CHK1 intrinsic activity and pS296, in contrast to stress-related pS317 or pS345 (Bass and Cortez, 2019; Haahr et al., 2016; Michelena et al., 2019). These data show that TRESLIN depletion can trigger the bypass of S-phase despite elevated

Figure 2. TRESLIN-depleted cells are in a premature G2 steady state facilitated by WEE1 activities

(A and B) QIBC of HeLa cells transfected the indicated siRNAs (48 h) stained for cyclin E1 (A), cyclin A2 (B), and DAPI.

(C) Quantification of the indicated markers from cells in (A), (B), and Figure 1D. G2- and S-phase populations were identified as depicted in Figure 1B. Middle lines indicate medians, thick boxes indicate lower (25th, Q1) and upper (75th, Q3) quartiles, whiskers at 10 and 90 percentiles. n = 2,000. Values are from a single experiment representative of >3 independent experiments. a.u.; arbitrary units.

(D) HeLa cells transfected with the indicated siRNAs (48 h) and stained for the indicated markers (left panel). Scale bar is 10 μm. Quantification of nuclear H3-pS10 in S or G2 cells (n = 2,000) from the left panel (right panel). Boxplot parameters similar to (C).

(E) QIBC of HeLa cells expressing mTurquoise2-SLBP(18–126) transfected with the indicated siRNAs (48 h). Representative of 2 independent experiments.

(F) Immunoblot of extracts from HeLa cells transfected as in (A), where CDK2 or CDK1 were immunoprecipitated. pY15 levels were quantified relative to CDK2 or CDK1 and siCTR values.

(G) Immunoblot of whole-cell extracts (WCE) from HeLa cells transfected as in (A) and treated with 500 nM WEE1 inhibitor. pY15 levels were quantified relative to loading control H3 and normalized to lane 1.

(H) QIBC of HeLa cells transfected as in (A) were treated with DMSO or 500 nM WEE1 inhibitor for 2 h and stained for H3-pS10 and DAPI. Percentages indicate cells in mitosis (in red). See also Figure S2F.

(I) Images of cells transfected and treated as in (H) stained for the indicated markers. Scale bar is 20 μm.

(J) Boxplot quantification (as in C) of the indicated markers from cells treated as in (I). H3-pS10 positive cells identified as in (H) (in red). Boxplot parameters similar to (C). >50 cells are analyzed in each condition.

All QIBC data are representative of ≥3 independent biological replicates (unless specified).

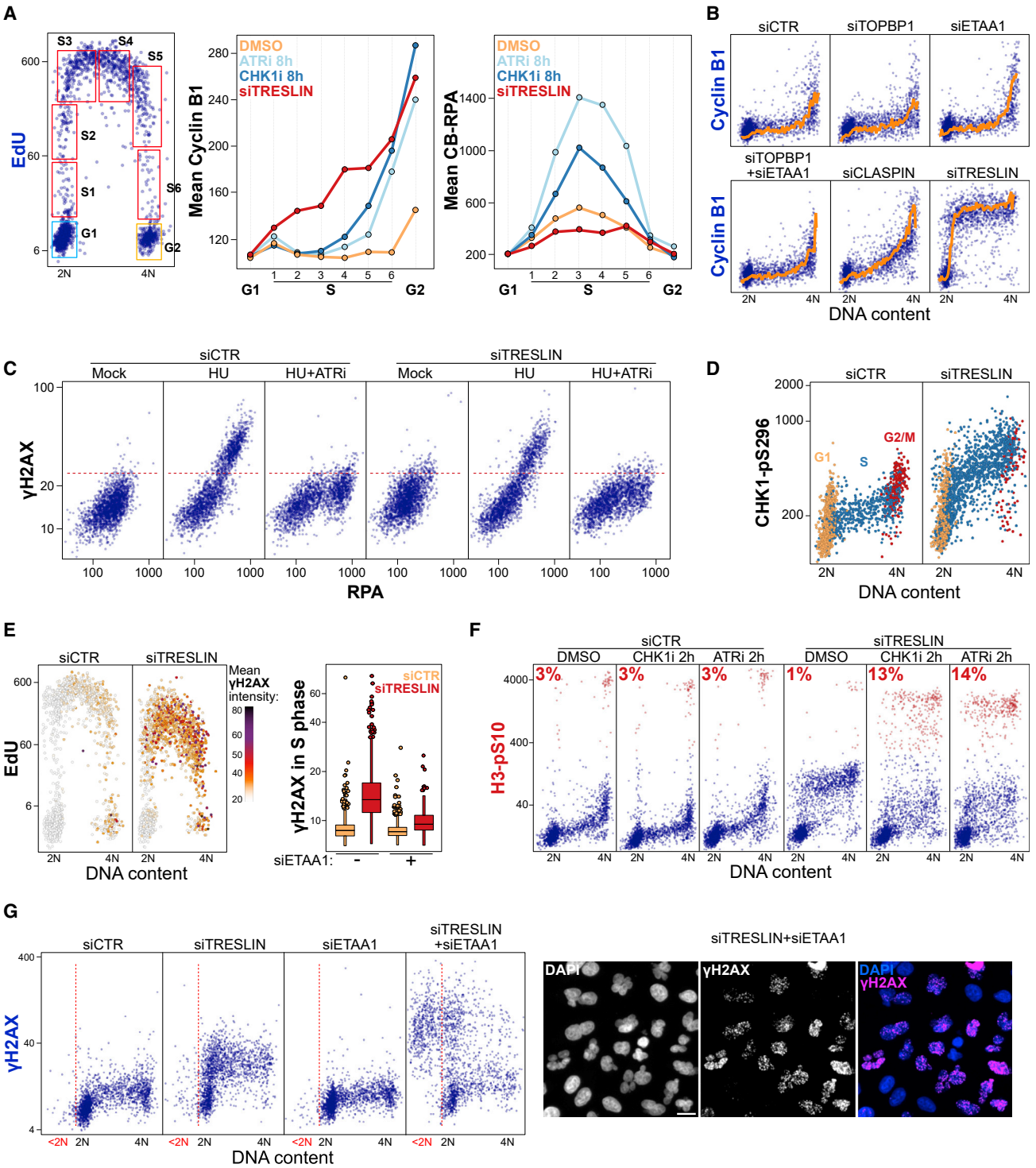

Figure 3. TRESLIN regulates the cell cycle independently of ATR and CHK1

(A) HeLa cells were transfected with the indicated siRNAs (48 h) and stained for EdU, cyclin B1, CB-RPA, and DAPI. CHK1 inhibitor (500 nM) or ATR inhibitor (2 μM) were applied for 8 h (blue, light blue lines). QIBC of EdU and DAPI stainings were used to identify different cell-cycle populations (left panel). Lines indicate mean intensities of the different populations (n = 2,000). Values shown from a single experiment representative of 3 independent experiments.

(B) QIBC of HeLa cells transfected with the indicated siRNAs (48 h) and stained for cyclin B1 and DAPI. Lines indicate population medians of cyclin B1 intensity in cells binned by DNA content (DAPI).

(legend continued on next page)

ATR activity, which thus far has been considered the key mechanism to delay cell cycle progression.

We reasoned that ATR/CHK1 signaling could be restraining CDK1 activity and mitotic entry in siTRESLIN cells. Indeed, CHK1 inhibition rapidly reduced CDK1-pY15 levels (Figure S3F) and, as ATRi, caused siTRESLIN cells to enter mitosis prematurely (<4n DNA) (Figures 3F and S3G). CHK1 inhibition caused a quick upregulation of CDC25B and a reduction in WEE1 phosphorylation (Figure S3H), previously shown to be important for its activity in *Xenopus* (Lee et al., 2001). Both events provide a mechanistic link to CDK1 activation upon ATR/CHK1 inhibition. Strikingly, ETAA1 depletion in siTRESLIN cells led to a massive accumulation of fragmented nuclei (sub-G1) with high levels of γH2AX, indicative of aberrant and/or premature mitosis (Figure 3G). Together, these data indicate that TRESLIN and ATR/CHK1 serve complementary functions in cell-cycle control. Although ATR/CHK1-mediated CDK repression is important for delaying the transition to mitosis, TRESLIN-MTBP masters the coordination between DNA replication and G2 entry.

TRESLIN function, and not DNA synthesis, prevents a premature entry into G2

In the light of the current model (Lemmens et al., 2018), we checked whether the premature entry into G2 in siTRESLIN cells is a consequence of impairing DNA synthesis. For this, we progressively depleted TRESLIN by titrating siRNA (Figure S4A). Surprisingly, the levels of cyclins (A2, B1, and E1), H3-pS10, and CDK activity were already affected in conditions where DNA synthesis was largely unaltered (Figures 4A–4D and S4B–S4D). By contrast, knockdown of other major regulators of DNA synthesis such as Timeless, POLE, or PCNA had no effect on cell-cycle markers despite causing a reduction in EdU incorporation as 5 nM siTRESLIN (Figures 4E and S4E). Together, these results indicate that TRESLIN's control of the cell cycle is not linked to levels of DNA synthesis. Interestingly, TRESLIN presence could halt the progression of the cell cycle even in conditions where DNA synthesis was fully blocked. Although 24 h thymidine arrest led to prematurely high CDK activity and cyclin A2 levels in S-phase (Figures 4F and S4F), cyclin B1 levels did not significantly change (Figures 4G and S4G), and thymidine-arrested cells did not enter mitosis upon WEE1 inhibition (Figure 4H). In contrast, thymidine-arrested siTRESLIN cells still entered mitosis upon WEE1 inhibition (Figure 4H). These data indicate that TRESLIN is responsible for tightly linking cell-cycle progression with DNA replication irrespectively of DNA synthesis levels. Interestingly, the fact that TRESLIN depletion affects cell-cycle progression more severely than it does DNA replication suggests the existence of different TRESLIN pools and that a large fraction of it is necessary to halt the transition into G2.

CDC7 activity regulates TRESLIN-MTBP recruitment to origins and prevents a premature S/G2 transition

Our data indicate that TRESLIN-MTBP monitors the progression of DNA replication. One potential monitoring mechanism could be that TRESLIN stability is linked to DNA replication, and protein levels are critically low at the end of S-phase, causing G2-entry. By synchronizing cells, we could see that TRESLIN levels were highest in G1 and rapidly dropped as cells entered S-phase (Figures 5A and S5A). To analyze this more quantitatively and to avoid the thymidine arrest, we generated a cell line stably expressing a TRESLIN-GFP fusion and quantified its levels using QIBC. As reported recently (Wittig et al., 2021), TRESLIN-GFP levels dropped after G1 but increased mildly throughout S and G2 phases, indicating that G2 entry is not directly linked to TRESLIN protein levels (Figure 5B). Since TRESLIN is recruited to DNA to promote origin firing, we explored whether its chromatin-bound (CB) pool could be acting as a molecular counter of remaining preRCs to control the checkpoint. CB-TRESLIN and CB-MTBP levels peaked in G1 and rapidly decreased as cells entered S-phase (Figures 5A, 5B, and S5E). This contrasted with CDC45 or PCNA, which travel with active replication forks and therefore are highest in S-phase (Figures 5A and S5B). CB-MCMs marking remaining preRCs were high at the beginning of S-phase and sharply decreased until G2 (Figure S5C). In contrast, CB-TRESLIN-GFP levels were low and relatively stable throughout S-phase (Figure 5B), suggesting that these do not directly translate the levels of remaining preRCs.

We then hypothesized that TRESLIN could be implementing a dynamic system to monitor DNA replication during origin firing. To test this, we inhibited DBF4-dependent kinase (DDK), which is necessary for origin firing and, in budding yeast, is essential to recruit Sld3 (TRESLIN homolog) to phosphorylated MCMs (Deegan et al., 2016). Inhibition of CDC7 (kinase subunit of DDK) reduced MCM2 phosphorylation (Figure S5D), TRESLIN and MTBP chromatin binding (Figures 5C and S5E), and led to a reduction of DNA synthesis in an ATR/ETAA1-mediated arrest in late S-phase (Rainey et al., 2020) (Figure 5D). Similar to siTRESLIN, CDC7i-treated cells showed premature G2 entry, with high cyclin B1, H3-pS10, and CDK activity (Figures 5E, 5F, and S5F) as cells progressed into S-phase (Figures 5E and 5F). Interestingly, ETAA1 depletion in CDC7i treated cells completely alleviated the DNA-synthesis arrest (Figure 5D) but did not alter the induction of cyclin B1, H3-pS10, or CDK activity (Figures 5G and S5F). This reinforces the notion that the premature transition to

(C) QIBC of HeLa cells transfected with the indicated siRNAs (48 h) and stained for CB-RPA and γH2AX. Cells were treated with 2 mM hydroxyurea (HU) for 2 h. DMSO or 2 μM ATR inhibitor were added for the last 45 min. Stained for CB-RPA and γH2AX.
(D) QIBC of HeLa cells transfected with the indicated siRNAs (48 h) and stained for EdU, CHK1-pS296, and DAPI. Cell-cycle stages were tagged as in Figure 1B.
(E) QIBC of HeLa cells transfected with the indicated siRNA(s) for 48 h and stained for EdU, γH2AX, and DAPI. QIBC of control and TRESLIN-depleted cells (left panel). Color legend explained in methods. Boxplot of average γH2AX levels in EdU-positive cells (right panel), visualized as in Figure 2C, and >1,000 cells are analyzed in each condition.
(F) QIBC of HeLa cells transfected with control or TRESLIN siRNA for 48 h. Last 2 h, cells were treated with DMSO, 1 μM CHK1, or 2 μM ATR inhibitor. Stained for H3-pS10 and DAPI.
(G) QIBC of cells treated as in (E) (left panel). Representative images of TRESLIN + ETAA1 depleted cells stained for DAPI and γH2AX. Scale bar is 20 μm.
CTR, control. QIBC data are representative of ≥3 independent biological replicates.

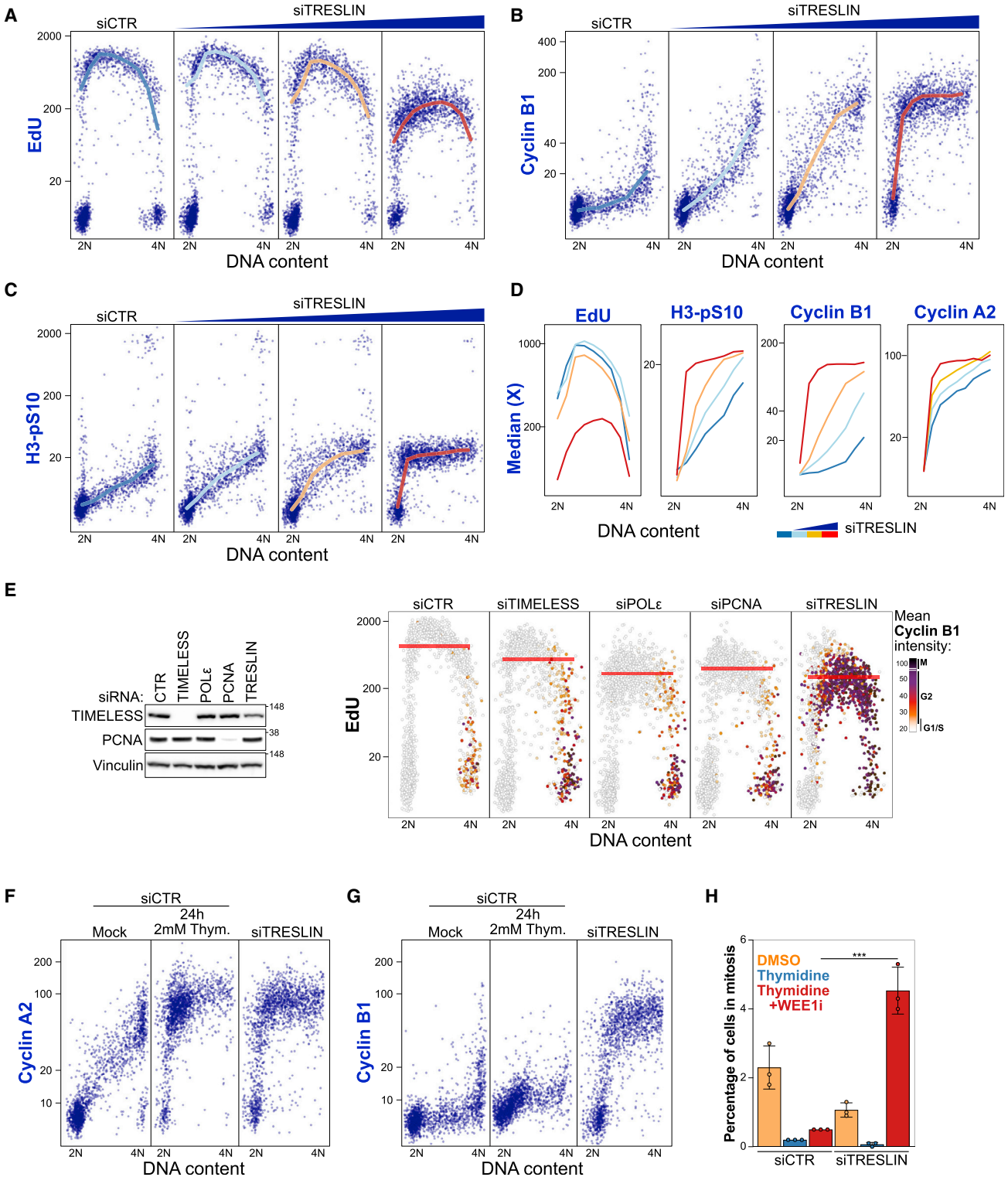

Figure 4. TRESLIN couples DNA replication with S/G2 transition independently of DNA synthesis

(A–C) QIBC of HeLa cells harboring CDK1/2 reporter transfected with control or TRESLIN siRNA (0.6, 1.25, or 5 nM) for 48 h. Stained for EdU, cyclin B1, H3-pS10, or cyclin A2 (see Figure S4C) and DAPI.

(D) Lines indicate median staining intensity of cells binned by DAPI values from (A) to (C), and Figure S4C.

(legend continued on next page)

G2 is triggered independently of DNA replication. Depletion of RIF1, which counteracts CDC7 activity (Alver et al., 2017; Hiraga et al., 2017) (Figure S5D), caused an increase in CB-TRESLIN-GFP levels and an opposite phenotype to CDC7 inhibition, namely elevated DNA synthesis and decreased CDK activity (Figures 5H–5J). Importantly, the increase in CB-TRESLIN-GFP caused by RIF1 depletion was quickly reversed by CDC7i (Figure 5H). Together, these data suggest that TRESLIN's control of the S/G2 transition depends on its ability to access chromatin and origins of replication via CDC7 signaling.

CDC45-mediated release of TRESLIN-MTBP from preRCs is required for the S/G2 checkpoint

In addition to CDC7 activity, TRESLIN requires phosphorylation by CDK2 on T969 and S1001 to facilitate TOPBP1 binding and origin firing (Boos et al., 2011; Kumagai et al., 2011). Interestingly, expression of an siRNA-resistant double T969A/S1001A mutant (TRESLIN^{TASA}) failed to rescue either DNA replication levels or the premature G2-entry after TRESLIN depletion (Figures S6A and S6B). This suggests that origin firing activity downstream of TRESLIN is important for its control of the cell cycle. Since TOPBP1 depletion failed to reproduce the effect of TRESLIN knockdown (Figure 3B), we depleted CDC45 instead, the major regulator of origin firing downstream of TRESLIN that also requires TRESLIN phosphorylations to be incorporated into active CMGs (Ferreira et al., 2022). CDC45 depletion caused a reduction in DNA synthesis and the cell's capacity to support origin firing, which was measured by the accumulation of RPA on chromatin (a surrogate of active forks) induced by ATR inhibition (Figure S6C) (Toledo et al., 2013). Similar to TRESLIN, CDC45 knockdown caused a premature G2 state with elevated cyclin B1, which was rescued by exogenous expression of CDC45 (Figures 6A and S6D). CDK activity, H3-pS10, and mitotic entry after WEE1 inhibition were also elevated (Figures S6E and S6F). According to our data with CDC7i, this could indicate that CDC45 depletion impairs TRESLIN-MTBP access to preRCs. Strikingly, however, CDC45 depletion led to a large increase in the levels of TRESLIN and MTBP on chromatin across S-phase (Figures 6B, 6C, and S6G–S6I), which was dependent on CDC7 (Figures 6C, S6G, and S6H) and also rescued by reintroduction of CDC45 (Figure S6J). It was evident that in the absence of CDC45, TRESLIN-GFP was concentrated at preRCs (MCMs), particularly at the end of S-phase (Figure 6D). TRESLIN^{TASA} was also retained on chromatin after CDC45 or endogenous TRESLIN depletion, supporting that CDC45 recruitment and/or other events downstream are necessary for TRESLIN release from preRCs (Figure S6K). To check the latter possibility, we depleted other proteins involved in origin firing, such as RECQ4 and GINS1 (Figure S6L). In contrast to CDC45, depletion of these factors did not cause a premature cyclin B1 expression or an accumulation of CB-TRESLIN, despite severely affecting the cell's capacity for origin firing (Figures 6E, 6F, and S6M). Together with Figure 5, these data suggested that for the S/G2 checkpoint to function, TRESLIN-MTBP must be recruited to preRCs (via CDC7) and subsequently released upon the action of CDC45. Consistently, TRESLIN and CDC45 location on chromatin was nearly mutually exclusive, with CB-TRESLIN absent from active replication forks (marked by CB-PCNA) (Figure 6G). These observations would underpin a system to monitor S-phase progression where the dynamic turnover of TRESLIN-MTBP with CDC45 at preRCs is considered the molecular evidence of the execution of origin firing. Interestingly, the nucleoplasmic levels of TRESLIN were higher in siCDC45 and CDC7i-treated cells, both conditions where the checkpoint was inactive (Figure 6H). This would argue again that the checkpoint is not maintained simply by TRESLIN protein levels but by a specific pool generated after CDC45-mediated release from preRCs, potentially marked by transient post-translational modifications (see discussion).

TRESLIN-MTBP monitors the rate of origin firing to determine the end of S-phase

In this manner, TRESLIN-MTBP would be able to sense the rate of origin firing quantitatively, keeping the checkpoint ON when origin firing is high and turning it OFF when origin firing falls below a threshold that marks the end of S-phase. To test this, we gradually depleted CDC45 to reduce the cell's capacity to support origin firing, thereby mimicking the end of DNA replication. Expectedly, as we deplete more CDC45 (Figure 7A, from left to right in the panel), the cells capacity to fire origins got reduced progressively. Interestingly, the levels of both CB-TRESLIN-GFP and cyclin B1 started increasing only when CDC45 depletion caused origin firing capacity to reach a minimum, a situation potentially resembling the end of S-phase (Figures 7A and S7A). Similar values were observed for CB-MTBP-GFP (Figure S7B). Supporting this, we observed that cells entering the latest stage of S-phase suffered a sudden decrease in origin firing capacity, similar to a strong CDC45 depletion (Figures 7B and S7C). The few TRESLIN molecules left on chromatin in late S (Figure 5B) were concentrated within MCM2 clusters, also a sign of impaired origin firing (Figures 7C and S7D). We thus propose that TRESLIN-MTBP monitors the precipitous decline of origin firing at the end of S-phase, which serves as the switch to trigger entry into G2 (Figure 7D).

DISCUSSION

Our data show that the TRESLIN-MTBP complex simultaneously holds the control for promoting DNA replication and for

(E) Immunoblotting of extracts from HeLa cells transfected with the indicated siRNA (48 h) (left panel). QIBC of HeLa cells stained for EdU, cyclin B1, and DAPI (right panel). siCTR, siPCNA and siTRESLIN (n = 3), and siTIMELESS and siPOLE (n = 2). Red lines indicate average mean EdU intensity in S-phase. Color legend explained in STAR Methods.

(F and G) QIBC of HeLa cells harboring CDK1/2 reporter transfected with the indicated siRNAs (48 h). Last 24 h, cells were left untreated or treated with 2 mM thymidine (Thym.). Stained for cyclin A2 (F) or cyclin B1 (G).

(H) Cells treated as in (F) and (G). 500 nM WEE1 inhibitor was added for 2 h before collection. Cells were stained for H3-pS10 and DAPI. Mean percentage of H3-pS10 positive cells is shown for three independent replicates. Error bars = SD. ***$p \leq 0.0005$, unpaired t test.

CTR, control. All QIBC data are representative of $\geq$3 independent biological replicates (unless specified otherwise).

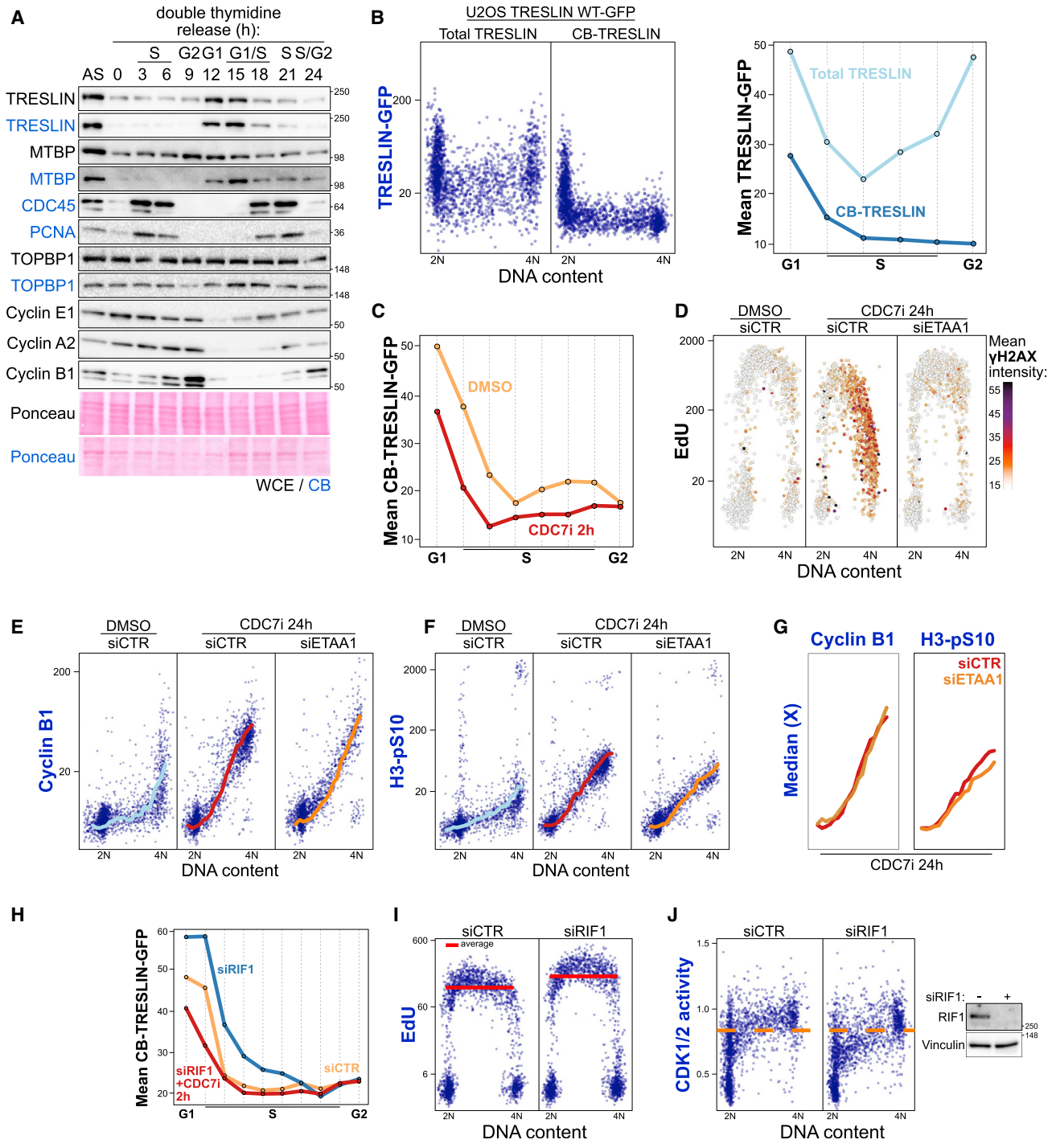

Figure 5. CDC7 activity promotes TRESLIN-MTBP recruitment to origins and prevents a premature S/G2 transition

(A) HeLa cells were released from a double thymidine block (2 mM) (18 h ON, 9 h release, 15 h ON) and collected for immunoblotting every 3 h. WCE and CB extracts were analyzed. TOPBP1 was used as loading control.

(B) QIBC (left panel) of U2OS cells harboring TRESLIN WT-GFP construct. Cells were either fixed or pre-extracted to study total and chromatin levels of TRESLIN, respectively. Mean intensity of TRESLIN WT-GFP signal was quantified in different cell-cycle stages as in Figure 1B (n = 2,000). Single experiment representative of >3 independent experiments.

(C) U2OS cells harboring TRESLIN WT-GFP were treated with DMSO or 10 μM CDC7 inhibitor (CDC7i) (2 h). 10 μM EdU was added for the last 30 min, and cells were pre-extracted prior fixation. Cell-cycle stages were tagged as in Figure 1B. Mean intensities (n = 2,000) are shown from a single experiment representative of 3 independent experiments.

(legend continued on next page)

restraining entry into G2 until the genome has been duplicated. We show how these two functions are linked at an early step of origin firing, where CDC7 recruits TRESLIN-MTBP to preRCs, and CDC45 and CDK activity promotes its subsequent release (Figure 7D). This allows the cell to promote and monitor origin firing simultaneously. Accordingly, proteins involved in origin firing downstream of this step (TOPBP1, RECQ4, GINS, and POLE) are dispensable for the checkpoint function (Douglas et al., 2018). In contrast, a partial depletion of TRESLIN already affects the checkpoint without a measurable effect on DNA replication. This indicates that although a few TRESLIN molecules may suffice to support a substantial rate of origin firing (suggesting some mechanism of recycling), a higher number needs to accumulate to maintain the checkpoint active.

The principles of our S/G2 checkpoint model emerge when we compare it with the spindle assembly checkpoint (SAC) (Lara-Gonzalez et al., 2021). The SAC detects unattached kinetochores, where the rapid conversion of free *open*-Mad2 to a closed conformation traps the APC/C activator CDC20, forming the mitotic checkpoint complex (MCC). To prohibit aneuploidy, one unattached kinetochore suffices to produce enough MCC molecules to keep the SAC ON. The S/G2 checkpoint uses origins as the unattached kinetochores, but it has evolved to require a high rate of origin firing to ensure a sufficient pool of inhibitory TRESLIN-MTBP. In turn, rather than checking for the very last origin to fire (as the SAC does), it relies on a decline in the rate of origin firing that only happens in very late S, which seems a reasonable compromise. First, it would be challenging to have a system sensitive enough to detect the very last fired origin (when cells normally have thousands of active forks at any given time). Second and most importantly, this would not be a necessary condition since entering G2 or even mitosis with unreplicated DNA does not pose a lethal threat, as cells have evolved to deal with this during G2, mitosis, and even post cytokinesis (Minocherhomji et al., 2015; Mocanu et al., 2022; Spies et al., 2019).

Our data contrast with the current model for S/G2 transition, by which the ATR/CHK1 pathway translates DNA replication into a "cell-cycle brake" that is switched off when the last replication forks terminate (Lemmens and Lindqvist, 2019; Lemmens et al., 2018; Saldivar et al., 2018). It is expected that chemical inhibition of ATR/CHK1 will enhance CDK1/2 activity and accelerate the S/G2/M transition to a certain extent. However, it is unclear whether ATR/CHK1 are inactivated to such an extent in physiological conditions, when cells stop replicating DNA (Saldivar et al., 2018). For instance, ATR/CHK1 play a key in the DNA damage-induced G2/M checkpoint (Liu and Guntuku, 2000; Lukas et al., 2004; Stiff et al., 2008), and both our data and recent evidence show intrinsic ATR/CHK1 activity in G2 and mitosis (Bass and Cortez, 2019; Kabeche et al., 2018; Michelena et al., 2019). It is also unclear how such a checkpoint would be regulated in the presence of persistent RS markers (Daigh et al., 2018) or whether ssDNA levels are sufficient to establish the dynamic window that discriminates between S and G2 (Ercilla et al., 2020). Additionally, the ATR intrinsic checkpoint has been proposed to be controlled by ETAA1 monitoring RPA bound to ssDNA, and yet ETAA1-deleted cells are viable (Bass et al., 2016; Haahr et al., 2016; Saldivar et al., 2018).

Our work introduces a new perspective for mammalian cell-cycle control, proposing that TRESLIN-MTBP and ATR/CHK1 have complementary roles in controlling S/G2/M transition. At the end of S-phase, the TRESLIN-MTBP origin firing checkpoint facilitates the transition to a phase with intermediate CDK1 activity (G2). Meanwhile ATR/CHK1, and later WEE1, limits CDK1 hyper-activation, acting as a safe-lock mechanism that minimizes the risk of premature mitotic entry. Our data support that ATR activation is achieved via ETAA1 stimulation by hyperactive CDKs in the absence of TRESLIN (Achuthankutty et al., 2019), suggesting that ETAA1 could be acting as a sensor for CDK activity that implements a negative feedback loop enabling a safe S to M transition. Additionally, this could explain why ETAA1 becomes essential to prevent premature mitosis in the absence of TOPBP1, a condition with impaired ATR and possible premature CDK activation (Bass et al., 2016; Haahr et al., 2016).

How CDK1/2 are hyperactive in S-phase cells upon TRESLIN depletion independently of ATR/CHK1 remains to be explored. The high CDK1-pY15 levels in siTRESLIN cells (despite elevated CDC25A, B, and C, Figure S3H) favor a CDC25-independent mechanism for elevating CDK activity. Cyclin A2 plays an important role in maintaining CDK activity levels, but these also rise in a subset of siTRESLIN cells in a cyclin A2 independent manner. Importantly, although high cyclin A2 and high CDK activity are necessary to cause a premature G2, they are not sufficient (Figures 4F and 4G). This highlights that the CDC7-TRESLIN-MTBP imposes an extra degree of regulation that holds the key to G2 entry, ensuring that the expression of pro-mitotic cell cycle regulators is suppressed even if CDK activity is aberrantly high.

Limitations of the study

Although we describe the coordinated action of CDC7, TRESLIN-MTBP, and CDC45 at replication origins to regulate the S/G2 checkpoint, we cannot discard that additional functions of these proteins are also at play for checkpoint control, independently of origin firing. Likewise, different mechanistic aspects of the S/G2 checkpoint remain to be dissected, which were beyond

(D–G) HeLa cells were transfected with the indicated siRNAs (48 h) and treated with DMSO or 10 μM CDC7i for the last 24 h. QIBC of EdU and γH2AX (D), cyclin B1 (E), and H3-pS10 (F). Cyclin B1 data in untreated siCTR (E) are also used in Figure 3B. Lines indicate median staining intensity of cells binned by DAPI values (G). Color legend explained in methods (D).

(H and I) U2OS cells harboring TRESLIN WT-GFP construct were transfected with the indicated siRNAs (48 h). Cells were either left untreated or treated with 10 μM CDC7i (2 h) (H). Mean CB-TRESLIN WT-GFP signal was quantified in different cell-cycle stages as in Figure 1B (n = 2,000). Single experiment values representative of 3 independent experiments. QIBC of EdU intensity in control or RIF1 siRNA treated cells (I). Red line indicates mean EdU intensity in S-phase.

(J) QIBC (left panel) of HeLa cells harboring CDK1/2 reporter were transfected with the indicated siRNAs (48 h). Dotted line as reference. Immunoblotting of transfected Hela cells confirming RIF1 depletion (right panel).

CTR, control. QIBC data are representative of ≥3 independent biological replicates.

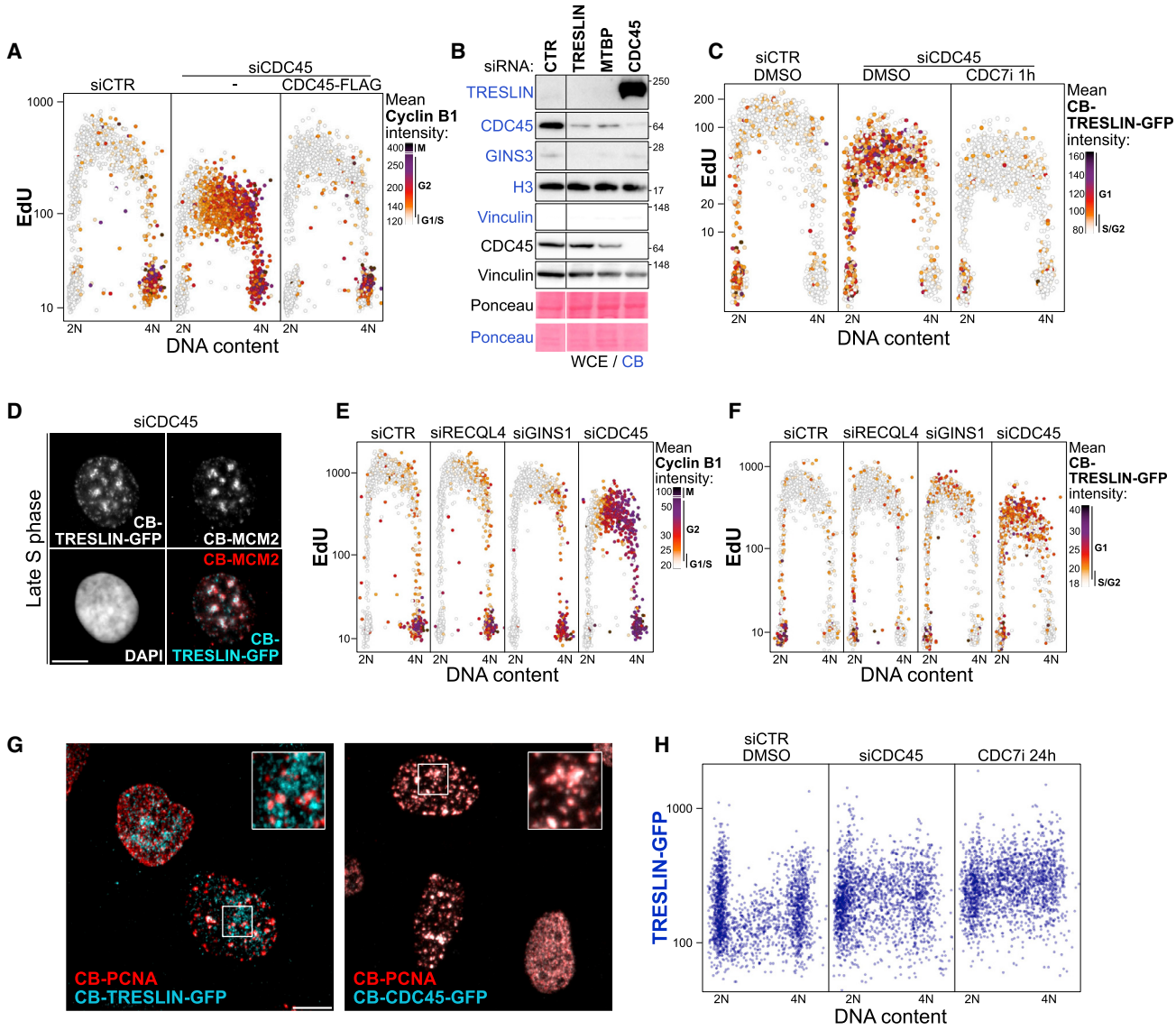

Figure 6. CDC45-mediated release of TRESLIN-MTBP from preRCs is required for the S/G2 checkpoint

(A) QIBC of U2OS cells harboring TRESLIN WT-GFP and CDC45-3xFLAG constructs transfected with control or CDC45 siRNA for 72 h. Stained for cyclin B1, EdU, and DAPI. Color legend explained in STAR Methods.

(B) Immunoblot of whole-cell (WCE) or CB extracts from HeLa cells transfected with indicated siRNAs (48 h). Histone H3 and vinculin were used as loading control. Blot is split to exclude irrelevant samples.

(C) QIBC of U2OS cells harboring TRESLIN WT-GFP construct treated as in (A) were treated with DMSO or 10 μM CDC7i for 1 h. Cells were pre-extracted and stained for GFP, EdU, and DAPI. Color legend explained in STAR Methods.

(D) Representative images of cells treated as in (C), pre-extracted and stained for GFP, EdU, MCM2, and DAPI. Late S-phase was identified by EdU and DAPI staining. Scale bar is 10 μm.

(E and F) QIBC of U2OS cells harboring TRESLIN WT-GFP construct transfected with indicated siRNAs for 72 h. Stained for EdU, cyclin B1, GFP, and DAPI. Color legend explained in STAR Methods.

(G) Confocal images of U2OS cells harboring TRESLIN WT-GFP construct (left) or endogenously tagged CDC45 (right), pre-extracted, and stained for PCNA to mark active replication forks. Scale bar is 10 μm.

(H) QIBC of U2OS cells harboring TRESLIN WT-GFP construct transfected with control or CDC45 siRNA for 72 h. Cells were treated with DMSO or 10 μM CDC7 inhibitor for the last 24 h. Stained for GFP and DAPI.

QIBC data are representative of ≥3 independent biological replicates.

the scope of this study. Further work is required to show TRESLIN-MTBP transient role at origins and its connection with CDC45, for instance taking advantage of *in vitro* systems recently developed in other species (i.e., in *Xenopus* or yeast). Better tools to detect endogenous TRESLIN-MTBP would also help us understand its dynamics in human cells. As highlighted

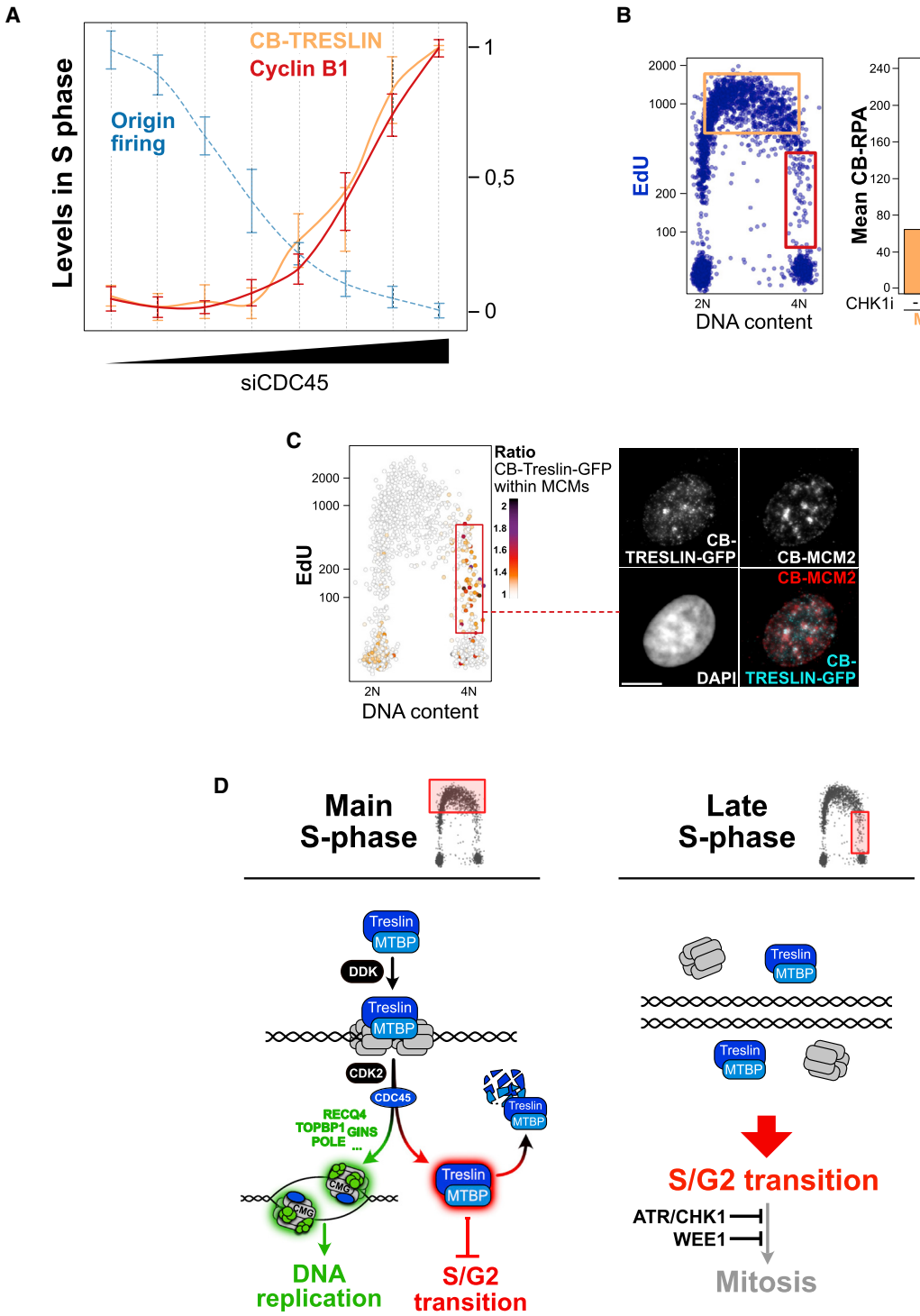

Figure 7. TRESLIN monitors origin availability to control S/G2 transition

(A) Median intensities of CB-RPA32 (blue dotted line), cyclin B1, and CB-TRESLIN-GFP in U2OS cells harboring TRESLIN WT-GFP, transfected with control or CDC45 siRNA (10 nM, 1 → 0.03 nM—1:2 dilutions) for 72 h. To measure origin firing (CB-RPA32), cells were treated with 2 μM ATR inhibitor for 3 h. Cells were pre-extracted for CB-RPA32 and CB-TRESLIN. Lines show mean and SD of 3 independent experiments (n = 2,000 in each experiment).

(B) QIBC of U2OS cells stained for EdU (left panel) and CB-RPA (right panel). Cells were treated with 1 μM CHK1 inhibitor for 60 min, mean intensities are shown from a single experiment representative of 3 independent experiments.

(C) QIBC (left panel) of U2OS cells harboring TRESLIN WT-GFP pre-extracted and stained for EdU, TRESLIN-GFP, and MCM2. Representative image (right panel) of late S-phase cells, stained for TRESLIN-GFP, MCM2, and DAPI. Scale bar is 10 μm.

(legend continued on next page)

in our model (Figure 7D), we propose that S/G2 checkpoint control relies on different pools (some transient) of TRESLIN-MTBP, likely marked by specific PTMs. Characterizing these may require extensive generation and analysis of TRESLIN-MTBP mutants combined with a MS-based profiling of their PTMs. Finally, a thorough comparative analysis of the interactome of TRESLIN-MTBP mutants could clarify how it regulates CDKs and other critical cell-cycle-promoting factors.

STAR★METHODS

Detailed methods are provided in the online version of this paper and include the following:

- KEY RESOURCES TABLE
- RESOURCE AVAILABILITY
  - Lead contact
  - Materials availability
  - Data and code availability
- EXPERIMENTAL MODEL AND SUBJECT DETAILS
  - Cell culture
  - Cell lines
- METHOD DETAILS
  - Cloning of FUW-CDC45-3xFLAG
  - Drugs and cell culture supplements
  - Gene silencing by siRNA
  - Immunostaining
  - Microscopy and Quantitative Image Based Cytometry (QIBC)
  - Chromatin and soluble fractionations
  - Immunoprecipitation
  - Immunoblotting
  - Mass Spectrometry - whole proteome sample preparation
  - Mass Spectrometry - LC-MS analysis
  - Mass Spectrometry data analysis
  - RNAseq library preparation and sequencing
  - RNA-seq data processing and analysis
- QUANTIFICATION AND STATISTICAL ANALYSIS

SUPPLEMENTAL INFORMATION

Supplemental information can be found online at https://doi.org/10.1016/j.molcel.2022.08.006.

ACKNOWLEDGMENTS

We thank Alexis Barr (Imperial College), Christopher Sansam (University of Oklahoma), and Niels Mailand (University of Copenhagen) for providing critical reagents. We thank Jiri Lukas, Ian Hickson, Julien Duxin (University of Copenhagen), and Kumar Somyajit (University of Southern Denmark) for revising and providing feedback on the manuscript. We thank David Willman with the assistance on immunoprecipitation studies and Justine Sitz for help with the confocal microscope. We thank everyone in the Toledo Laboratory for critical comments on the manuscript. Work at the Center for Chromosome Stability was supported by the European Research Council, European Union (ERC-StG-679754), and the Danish National Research Foundation, Denmark (DNRF115). Work at the University of Duisburg-Essen was supported by the NRW Rückkehrerförderprogramm fellowship. Work at the Novo Nordisk Foundation Center for Protein Research was supported by the Novo Nordisk Foundation (grant agreements NNF14CC0001 and NNF15CC0001).

AUTHOR CONTRIBUTIONS

G.Z. performed the experiments. G.Z. and L.T. designed and analyzed the experiments. R.V. and E.M.-D. developed reagents and provided input for the study. S.A. and J.B. carried out initial experiments. D.B. provided critical reagents, input, and advice during the study. F.C. and A.M. carried out mass spectrometry analysis. M.L. analyzed the RNA-seq dataset. L.T. conceived, designed, and supervised the study. L.T., G.Z., and R.V. wrote the manuscript. All of the authors read, edited, and commented on the manuscript.

DECLARATION OF INTERESTS

The authors declare no competing interests.

INCLUSION AND DIVERSITY

While citing references scientifically relevant for this work, we also actively worked to promote gender balance in our reference list.

Received: September 30, 2021
Revised: May 16, 2022
Accepted: August 4, 2022
Published: August 31, 2022

REFERENCES

Achuthankutty, D., Thakur, R.S., Haahr, P., Hoffmann, S., Drainas, A.P., Bizard, A.H., Weischenfeldt, J., Hickson, I.D., and Mailand, N. (2019). Regulation of ETAA1-mediated ATR activation couples DNA replication fidelity and genome stability. J. Cell Biol. *218*, 3943–3953. https://doi.org/10.1083/jcb.201905064.

Alver, R.C., Chadha, G.S., Gillespie, P.J., and Blow, J.J. (2017). Reversal of DDK-mediated MCM phosphorylation by Rif1-PP1 regulates replication initiation and replisome stability independently of ATR/Chk1. Cell Rep. *18*, 2508–2520.

Bajar, B.T., Lam, A.J., Badiee, R.K., Oh, Y.-H., Chu, J., Zhou, X.X., Kim, N., Kim, B.B., Chung, M., Yablonovitch, A.L., et al. (2016). Fluorescent indicators for simultaneous reporting of all four cell cycle phases. Nat. Methods *13*, 993–996.

Barr, A.R., Heldt, F.S., Zhang, T., Bakal, C., and Novák, B. (2016). A dynamical framework for the all-or-none G1/S transition. Cell Syst. *2*, 27–37.

Bass, T.E., and Cortez, D. (2019). Quantitative phosphoproteomics reveals mitotic function of the ATR activator ETAA1. J. Cell Biol. *218*, 1235–1249.

Bass, T.E., Luzwick, J.W., Kavanaugh, G., Carroll, C., Dungrawala, H., Glick, G.G., Feldkamp, M.D., Putney, R., Chazin, W.J., and Cortez, D. (2016). ETAA1 acts at stalled replication forks to maintain genome integrity. Nat. Cell Biol. *18*, 1185–1195.

Boos, D., Sanchez-Pulido, L., Rappas, M., Pearl, L.H., Oliver, A.W., Ponting, C.P., and Diffley, J.F.X. (2011). Regulation of DNA replication through

(D) Model for TRESLIN-MTBP monitoring origin firing. TRESLIN-MTBP complex is recruited to DDK-mediated phosphorylated MCM complexes (left panel). CDK2 and CDC45 loading simultaneously promote origin firing (green arrow), and TRESLIN-MTBP release (red arrow) independently of downstream replication factors. This form of released TRESLIN-MTBP (red) keeps the S/G2 checkpoint active and has a limited half-life. TRESLIN is subsequently degraded or potentially reused. This mechanism is switched off in late S-phase due to the scarcity of origins, triggering the S/G2 transition (right panel), whereas ATR/CHK1 cooperate to prevent premature mitotic entry.
QIBC data are representative of ≥3 independent biological replicates.

Sld3-Dpb11 interaction is conserved from yeast to humans. Curr. Biol. *21*, 1152–1157.

Boos, D., Yekezare, M., and Diffley, J.F.X. (2013). Identification of a heteromeric complex that promotes DNA replication origin firing in human cells. Science *340*, 981–984.

Brown, E.J., and Baltimore, D. (2000). ATR disruption leads to chromosomal fragmentation and early embryonic lethality. Genes Dev. *14*, 397–402.

Cox, J., Hein, M.Y., Luber, C.A., Paron, I., Nagaraj, N., and Mann, M. (2014). Accurate proteome-wide label-free quantification by delayed normalization and maximal peptide ratio extraction, termed MaxLFQ. Mol. Cell. Proteomics *13*, 2513–2526.

Cox, J., and Mann, M. (2008). MaxQuant enables high peptide identification rates, individualized p.p.b.-range mass accuracies and proteome-wide protein quantification. Nat. Biotechnol. *26*, 1367–1372.

Cox, J., Neuhauser, N., Michalski, A., Scheltema, R.A., Olsen, J.V., and Mann, M. (2011). Andromeda: a peptide search engine integrated into the MaxQuant environment. J. Proteome Res. *10*, 1794–1805.

Daigh, L.H., Liu, C., Chung, M., Cimprich, K.A., and Meyer, T. (2018). Stochastic endogenous replication stress causes ATR-triggered fluctuations in CDK2 activity that dynamically adjust global DNA synthesis rates. Cell Syst. *7*, 17–27.e3.

Deegan, T.D., Yeeles, J.T.P., and Diffley, J.F.X. (2016). Phosphopeptide binding by Sld3 links Dbf4-dependent kinase to MCM replicative helicase activation. EMBO J. *35*, 961–973.

Douglas, M.E., Ali, F.A., Costa, A., and Diffley, J.F.X. (2018). The mechanism of eukaryotic CMG helicase activation. Nature *555*, 265–268.

Ercilla, A., Benada, J., Amitash, S., Zonderland, G., Baldi, G., Somyajit, K., Ochs, F., Costanzo, V., Lukas, J., and Toledo, L. (2020). Physiological tolerance to ssDNA enables strand uncoupling during DNA replication. Cell Rep. *30*, 2416–2429.e7.

Eykelenboom, J.K., Harte, E.C., Canavan, L., Pastor-Peidro, A., Calvo-Asensio, I., Llorens-Agost, M., and Lowndes, N.F. (2013). ATR activates the S-M checkpoint during unperturbed growth to ensure sufficient replication prior to mitotic onset. Cell Rep. *5*, 1095–1107.

Fahrenkamp, D., de Leur, H.S.-V., Küster, A., Chatain, N., and Müller-Newen, G. (2015). Src family kinases interfere with dimerization of STAT5A through a phosphotyrosine-SH2 domain interaction. Cell Commun. Signal. *13*, 10.

Ferreira, P., Sanchez-Pulido, L., Marko, A., Ponting, C.P., and Boos, D. (2022). Refining the domain architecture model of the replication origin firing factor Treslin/TICRR. Life Sci. Alliance *5*, e202101088. https://doi.org/10.26508/lsa.202101088.

Fragkos, M., Ganier, O., Coulombe, P., and Méchali, M. (2015). DNA replication origin activation in space and time. Nat. Rev. Mol. Cell Biol. *16*, 360–374.

Gu, J., Xia, X., Yan, P., Liu, H., Podust, V.N., Reynolds, A.B., and Fanning, E. (2004). Cell cycle-dependent regulation of a human DNA helicase that localizes in DNA damage foci. Mol. Biol. Cell *15*, 3320–3332.

Haahr, P., Hoffmann, S., Tollenaere, M.A.X., Ho, T., Toledo, L.I., Mann, M., Bekker-Jensen, S., Räschle, M., and Mailand, N. (2016). Activation of the ATR kinase by the RPA-binding protein ETAA1. Nat. Cell Biol. *18*, 1196–1207.

Hassan, B.H., Lindsey-Boltz, L.A., Kemp, M.G., and Sancar, A. (2013). Direct role for the replication protein treslin (Ticrr) in the ATR kinase-mediated checkpoint response. J. Biol. Chem. *288*, 18903–18910.

Hendzel, M.J., Wei, Y., Mancini, M.A., Van Hooser, A., Ranalli, T., Brinkley, B.R., Bazett-Jones, D.P., and Allis, C.D. (1997). Mitosis-specific phosphorylation of histone H3 initiates primarily within pericentromeric heterochromatin during G2 and spreads in an ordered fashion coincident with mitotic chromosome condensation. Chromosoma *106*, 348–360.

Hiraga, S.-I., Ly, T., Garzón, J., Hořejší, Z., Ohkubo, Y.-N., Endo, A., Obuse, C., Boulton, S.J., Lamond, A.I., and Donaldson, A.D. (2017). Human RIF1 and protein phosphatase 1 stimulate DNA replication origin licensing but suppress origin activation. EMBO Rep. *18*, 403–419.

Kabeche, L., Nguyen, H.D., Buisson, R., and Zou, L. (2018). A mitosis-specific and R loop-driven ATR pathway promotes faithful chromosome segregation. Science *359*, 108–114.

Kelstrup, C.D., Bekker-Jensen, D.B., Arrey, T.N., Hogrebe, A., Harder, A., and Olsen, J.V. (2018). Performance evaluation of the Q Exactive HF-X for shotgun proteomics. J. Proteome Res. *17*, 727–738.

Koseoglu, M.M., Graves, L.M., and Marzluff, W.F. (2008). Phosphorylation of threonine 61 by cyclin A/Cdk1 triggers degradation of stem-loop binding protein at the end of S phase. Mol. Cell. Biol. *28*, 4469–4479.

Kulak, N.A., Geyer, P.E., and Mann, M. (2017). Loss-less nano-fractionator for high sensitivity, high coverage proteomics. Mol. Cell. Proteomics *16*, 694–705.

Kumagai, A., Shevchenko, A., Shevchenko, A., and Dunphy, W.G. (2010). Treslin collaborates with TopBP1 in triggering the initiation of DNA replication. Cell *140*, 349–359.

Kumagai, A., Shevchenko, A., Shevchenko, A., and Dunphy, W.G. (2011). Direct regulation of Treslin by cyclin-dependent kinase is essential for the onset of DNA replication. J. Cell Biol. *193*, 995–1007.

Labib, K., and De Piccoli, G. (2011). Surviving chromosome replication: the many roles of the S-phase checkpoint pathway. Philos. Trans. R. Soc. Lond. B Biol. Sci. *366*, 3554–3561.

Laoukili, J., Kooistra, M.R.H., Brás, A., Kauw, J., Kerkhoven, R.M., Morrison, A., Clevers, H., and Medema, R.H. (2005). FoxM1 is required for execution of the mitotic programme and chromosome stability. Nat. Cell Biol. *7*, 126–136.

Lara-Gonzalez, P., Pines, J., and Desai, A. (2021). Spindle assembly checkpoint activation and silencing at kinetochores. Semin. Cell Dev. Biol. *117*, 86–98. https://doi.org/10.1016/j.semcdb.2021.06.009.

Lee, J., Kumagai, A., and Dunphy, W.G. (2001). Positive regulation of Wee1 by Chk1 and 14-3-3 proteins. Mol. Biol. Cell *12*, 551–563.

Lemmens, B., Hegarat, N., Akopyan, K., Sala-Gaston, J., Bartek, J., Hochegger, H., and Lindqvist, A. (2018). DNA replication determines timing of mitosis by restricting CDK1 and PLK1 activation. Mol. Cell *71*, 117–128.e3.

Lemmens, B., and Lindqvist, A. (2019). DNA replication and mitotic entry: a brake model for cell cycle progression. J. Cell Biol. *218*, 3892–3902.

Liu, Q., Guntuku, S., Cui, X.S., Matsuoka, S., Cortez, D., Tamai, K., Luo, G., Carattini-Rivera, S., De Mayo, F., Bradley, A., et al. (2000). Chk1 is an essential kinase that is regulated by Atr and required for the G/M DNA damage checkpoint. Genes Dev. *14*, 1448–1459.

Lukas, J., Lukas, C., and Bartek, J. (2004). Mammalian cell cycle checkpoints: signalling pathways and their organization in space and time. DNA Repair *3*, 997–1007.

Maya-Mendoza, A., Petermann, E., Gillespie, D.A.F., Caldecott, K.W., and Jackson, D.A. (2007). Chk1 regulates the density of active replication origins during the vertebrate S phase. EMBO J. *26*, 2719–2731.

Michelena, J., Gatti, M., Teloni, F., Imhof, R., and Altmeyer, M. (2019). Basal CHK1 activity safeguards its stability to maintain intrinsic S-phase checkpoint functions. J. Cell Biol. *218*, 2865–2875.

Minocherhomji, S., Ying, S., Bjerregaard, V.A., Bursomanno, S., Aleliunaite, A., Wu, W., Mankouri, H.W., Shen, H., Liu, Y., and Hickson, I.D. (2015). Replication stress activates DNA repair synthesis in mitosis. Nature *528*, 286–290.

Mocanu, C., Karanika, E., Fernández-Casañas, M., Herbert, A., Olukoga, T., Özgürses, M.E., and Chan, K.-L. (2022). DNA replication is highly resilient and persistent under the challenge of mild replication stress. Cell Rep. *39*, 110701.

Moiseeva, T., Hood, B., Schamus, S., O'Connor, M.J., Conrads, T.P., and Bakkenist, C.J. (2017). ATR kinase inhibition induces unscheduled origin firing through a Cdc7-dependent association between GINS and And-1. Nat. Commun. *8*, 1392.

Moiseeva, T.N., Yin, Y., Calderon, M.J., Qian, C., Schamus-Haynes, S., Sugitani, N., Osmanbeyoglu, H.U., Rothenberg, E., Watkins, S.C., and Bakkenist, C.J. (2019). An ATR and CHK1 kinase signaling mechanism that limits origin firing during unperturbed DNA replication. Proc. Natl. Acad. Sci. USA *116*, 13374–13383.

Mueller, A.C., Keaton, M.A., and Dutta, A. (2011). DNA replication: mammalian Treslin-TopBP1 interaction mirrors yeast Sld3-Dpb11. Curr. Biol. *21*, R638–R640.

Muramatsu, S., Hirai, K., Tak, Y.-S., Kamimura, Y., and Araki, H. (2010). CDK-dependent complex formation between replication proteins Dpb11, Sld2, Pol (epsilon), and GINS in budding yeast. Genes Dev. *24*, 602–612.

Perez-Riverol, Y., Bai, J., Bandla, C., García-Seisdedos, D., Hewapathirana, S., Kamatchinathan, S., Kundu, D.J., Prakash, A., Frericks-Zipper, A., Eisenacher, M., et al. (2022). The PRIDE database resources in 2022: a hub for mass spectrometry-based proteomics evidences. Nucleic Acids Res. *50*, D543–D552.

Rainey, M.D., Bennett, D., O'Dea, R., Zanchetta, M.E., Voisin, M., Seoighe, C., and Santocanale, C. (2020). ATR restrains DNA synthesis and mitotic catastrophe in response to CDC7 inhibition. Cell Rep. *32*, 108096.

Roeschert, I., Poon, E., Henssen, A.G., Garcia, H.D., Gatti, M., Giansanti, C., Jamin, Y., Ade, C.P., Gallant, P., Schülein-Völk, C., et al. (2021). Combined inhibition of aurora-A and ATR kinase results in regression of MYCN-amplified neuroblastoma. Nat. Cancer *2*, 312–326.

Ruiz, S., Mayor-Ruiz, C., Lafarga, V., Murga, M., Vega-Sendino, M., Ortega, S., and Fernandez-Capetillo, O. (2016). A genome-wide CRISPR screen identifies CDC25A as a determinant of sensitivity to ATR inhibitors. Mol. Cell *62*, 307–313.

Sadasivam, S., Duan, S., and DeCaprio, J.A. (2012). The MuvB complex sequentially recruits B-Myb and FoxM1 to promote mitotic gene expression. Genes Dev. *26*, 474–489.

Saldivar, J.C., Hamperl, S., Bocek, M.J., Chung, M., Bass, T.E., Cisneros-Soberanis, F., Samejima, K., Xie, L., Paulson, J.R., Earnshaw, W.C., et al. (2018). An intrinsic S/G2 checkpoint enforced by ATR. Science *361*, 806–810.

Sansam, C.L., Cruz, N.M., Danielian, P.S., Amsterdam, A., Lau, M.L., Hopkins, N., and Lees, J.A. (2010). A vertebrate gene, ticrr, is an essential checkpoint and replication regulator. Genes Dev. *24*, 183–194.

Shechter, D., Costanzo, V., and Gautier, J. (2004). Regulation of DNA replication by ATR: signaling in response to DNA intermediates. DNA Repair *3*, 901–908.

Spencer, S.L., Cappell, S.D., Tsai, F.-C., Overton, K.W., Wang, C.L., and Meyer, T. (2013). The proliferation-quiescence decision is controlled by a bifurcation in CDK2 activity at mitotic exit. Cell *155*, 369–383.

Spies, J., Lukas, C., Somyajit, K., Rask, M.-B., Lukas, J., and Neelsen, K.J. (2019). 53BP1 nuclear bodies enforce replication timing at under-replicated DNA to limit heritable DNA damage. Nat. Cell Biol. *21*, 487–497.

Stiff, T., Cerosaletti, K., Concannon, P., O'Driscoll, M., and Jeggo, P.A. (2008). Replication independent ATR signalling leads to G2/M arrest requiring Nbs1, 53BP1 and MDC1. Hum. Mol. Genet. *17*, 3247–3253.

Syljuåsen, R.G., Sørensen, C.S., Hansen, L.T., Fugger, K., Lundin, C., Johansson, F., Helleday, T., Sehested, M., Lukas, J., and Bartek, J. (2005). Inhibition of human Chk1 causes increased initiation of DNA replication, phosphorylation of ATR targets, and DNA breakage. Mol. Cell. Biol. *25*, 3553–3562.

Toledo, L.I., Altmeyer, M., Rask, M.-B., Lukas, C., Larsen, D.H., Povlsen, L.K., Bekker-Jensen, S., Mailand, N., Bartek, J., and Lukas, J. (2013). ATR prohibits replication catastrophe by preventing global exhaustion of RPA. Cell *155*, 1088–1103.

Volpi, I., Gillespie, P.J., Chadha, G.S., and Blow, J.J. (2021). The role of DDK and Treslin-MTBP in coordinating replication licensing and pre-initiation Complex formation. Open Biol. *11*, 210121.

Wittig, K.A., Sansam, C.G., Noble, T.D., Goins, D., and Sansam, C.L. (2021). The CRL4DTL E3 ligase induces degradation of the DNA replication initiation factor TICRR/TRESLIN specifically during S phase. Nucleic Acids Res. *49*, 10507–10523. https://doi.org/10.1093/nar/gkab805.

Zeman, M.K., and Cimprich, K.A. (2014). Causes and consequences of replication stress. Nat. Cell Biol. *16*, 2–9.

STAR★METHODS

KEY RESOURCES TABLE

REAGENT or RESOURCE	SOURCE	IDENTIFIER
Primary antibodies		
BrdU	GE-Helthacare	Cat# RPN20AB
CDC45	Cell Signaling	Cat# 11881S
CDK1/2-pY15	Cell Signaling	Cat# 9111S
CDK1	BD Biosciences	Cat# 610037
CDK2	Santa Cruz	Cat# sc-6248
CHK1	Cell Signaling	Cat# 2360S
CHK1-pS296	Abcam	Cat# ab79758
CHK1-pS317	Cell Signaling	Cat# 2344S
CHK1-pS345	Cell Signaling	Cat# 2348S
CLASPIN	Santa Cruz	Cat# sc-376773
Cyclin A2 (B-8)	Santa Cruz	Cat# sc-271682
Cyclin B1 (GNS11)	Invitrogen	Cat# MA5-14327
Cyclin E1	Abcam	Cat# ab33911
ETAA1	Niels Mailand (Haahr et al., 2016)	N/A
FOXM1-pT600	Cell Signaling	Cat# 14655S
GAPDH	Novus Biologicals	Cat# NB600-502
GFP	Chromotek	Cat# PABG1-100
H2AX-pS139 (γH2AX) (JBW301)	Merck Millipore	Cat# 05-636
H3-pS10	Merck Millipore	Cat# 06-570
Histone H3	Abcam	Cat# ab1791
IgG	Merck Millipore	Cat# 12-371
MCM2 (6A8)	Novus Biologicals	Cat# H00004171-M01
MCM3	Santa Cruz	Cat# sc-390480
MCM7	Abcam	Cat# ab2360
MTBP (B-5)	Santa Cruz	Cat# sc-137201
PCNA (F-2)	Santa Cruz	Cat# sc-56
PCNA	Immunoconcepts	Cat# 2037
Pericentrin 1 (D-4)	Santa Cruz	Cat# sc-376111
RIF1	Cell Signaling	Cat# 95558S
RPA	Homemade (Ercilla et al., 2020)	N/A
RPA32 (9H8)	Novus Biologicals	Cat# NB600-565
TIMELESS	Abcam	Cat# ab109512
TOPBP1	Bethyl Laboratories	Cat# A300-111A-M
Treslin	Dominik Boos	N/A
Vinculin	Sigma-Aldrich	Cat# V9264-100UL
α-tubulin	Sigma-Aldrich	Cat# T6199-100UL
Secondary antibodies		
Alexa Fluor Plus 488 Goat anti-Mouse	Thermo Fisher	Cat# A32723
Alexa Fluor Plus 488 Goat anti-Rabbit	Thermo Fisher	Cat# A32731
Alexa Fluor Plus 555 Goat anti-Mouse	Thermo Fisher	Cat# A32727
Alexa Fluor Plus 555 Goat anti-Rabbit	Thermo Fisher	Cat# A32732
Alexa Fluor Plus 647 Goat anti-Mouse	Thermo Fisher	Cat# A32728
Alexa Fluor Plus 647 Goat anti-Rabbit	Thermo Fisher	Cat# A32733

(*Continued on next page*)

Continued

REAGENT or RESOURCE	SOURCE	IDENTIFIER
Anti-Mouse HRP	Sigma-Aldrich	Cat# A4416
Anti-Rabbit HRP	Sigma-Aldrich	Cat# A4416
Anti-Sheep HRP	Sigma-Aldrich	Cat# A3415
Bacterial and virus strains		
FUW-CDC45-3xFLAG	Addgene	Cat# 14882; 82990
mTurquoise-SLBP (18-126)	Addgene	Cat# 83842
Chemicals, peptides, and recombinant proteins		
Alexa Fluor 647 Azide,	Jena Bioscience	Cat# CLK-1299-1
AURORA A inhibitor (MLN8237)	Selleckchem	Cat# S1133
AZ20 (ATR inhibitor)	Selleckchem	Cat# S7050
AZD7762 (CHK1 inhibitor)	Selleckchem	Cat# S1532
Benzonase® Nuclease	Sigma-Aldrich	Cat# E1014-25KU
BI 2536 (PLK1 inhibitor)	Selleckchem	Cat# S1109
BrdU (5-Bromo-2′-deoxyuridine)	Sigma-Aldrich	Cat# B5002
BSA (Bovine serum Albumin)	Sigma-Aldrich	Cat# A7906
CDK2 inhibitor II	Calbiochem	Cat# 219445
DAPI (Diamidino-2-Phenylindole Dihydrochloride)	Sigma-Aldrich	Cat# D9542
DMSO (Dimethyl sulfoxide)	Sigma-Aldrich	Cat# D8418
Doxycycline	Sigma-Aldrich	Cat# D5207-1G
DTT (DL-Dithiothreitol)	Sigma-Aldrich	Cat# D0632
EdU (5-Ethynyl-2′-deoxyuridine)	Sigma-Aldrich	Cat# T511285
Formaldehyde 4%	VWR	Cat# 9713.1000
HU (Hydroxyurea)	Sigma-Aldrich	Cat# H8627
MK1775 (WEE1 inhibitor)	Selleckchem	Cat# S1525
Mowiol® 4-88	Sigma-Aldrich	Cat# 81381
Thymidine	Sigma-Aldrich	Cat# T1895
Vent® DNA Polymerase	New England Biolabs	Cat# M0254S
XL413 (CDC7 inhibitor)	AdooQ Bioscience	Cat# A21220
Deposited Data		
Raw Western Blot and Microscopy Data	Mendeley	https://doi.org/10.17632/8t7xh2ck55.1
RNAseq data	GEO	GSE210129
Mass Spectometry data	PRIDE	PXD035353
Experimental models: Cell lines		
Human: HeLa (female)	Laboratory of Ian Hickson	N/A
Human: HeLa CDK2L-GFP	Laboratory of Alexis Barr	https://pubmed.ncbi.nlm.nih.gov/27136687/
Human: HeLa Flp In T-Rex MTBP WT-3xFLAG-Tev2-GFP	Laboratory of Dominik Boos	https://pubmed.ncbi.nlm.nih.gov/30695077/
Human: HeLa Flp In T-Rex *wild-type*	Laboratory of Gerhard Müller-Newen	https://pubmed.ncbi.nlm.nih.gov/25885255/
Human: HeLa mTurquoise2-SLBP (18-126)	This paper	N/A
Human: hTERT-RPE1 (female)	ATCC	Cat# CRL-4000
Human: MCF7 (female)	Laboratory of Ian Hickson	N/A
Human: U2OS (female)	ATCC	Cat# HTB-96
Human: U2OS AcGFP-TRESLIN WT	Laboratory of Dominik Boos	https://pubmed.ncbi.nlm.nih.gov/23704573/
Human: U2OS AcGFP-TRESLIN WT CDC45-3xFLAG	This paper	N/A
Human: U2OS AcGFP-TRESLIN TASA	Laboratory of Dominik Boos	https://pubmed.ncbi.nlm.nih.gov/35091422/
Human: U2OS CDC45-GFP endogenously tagged	Laboratory of Jiri Lukas	https://pubmed.ncbi.nlm.nih.gov/33087936/
Human: U2OS Doxycycline-inducible TRESLIN WT and TASA mutant	Laboratory of Christopher Sansam	https://pubmed.ncbi.nlm.nih.gov/25737283/

(*Continued on next page*)

Continued

REAGENT or RESOURCE	SOURCE	IDENTIFIER
Oligonucleotides		
3xFLAG forward oligo with HpaI overhang: *5' GTCCTGGTTAACGACTACAAAGACCATGACGGTG ATTATAAAGATCATGACATCGACTACAAGGATGACG ATGACAAGTAGGAATTCGTCCTG 3'*	This paper	N/A
3xFLAG reverse oligo with EcoRI overhang: *5' CAGGACGAATTCCTACTTGTCATCGTCATCCTTGT AGTCGATGTCATGATCTTTATAATCACCGTCATGGTC TTTGTAGTCGTTAACCAGGAC 3'*	This paper	N/A
Mutagenesis forward primer for siRNA resistant CDC45: *5' CGTCAATGTATACAACGACACGCAAATCAAATTAC TCATTAAAC 3'*	This paper	N/A
Mutagenesis reverse primer for siRNA resistant CDC45: *5' GTTTAATGAGTAATTTGATTTGCGTGTCGTTGTATA CATTGACG 3'*	This paper	N/A
PCR forward primer for CDC45 with BamHI overhang: *5' CGAAGCGGATCCATGTTCGTATCCGATTTCCG 3'*	This paper	N/A
PCR reverse primer for CDC45 with HpaI overhang: *5' CGAAGCGTTAACGGACAGGAGGGAAATAAGTG 3'*	This paper	N/A
siRNA duplexes	This paper	See Table S1
Recombinant DNA		
FUW-CDC45-3xFLAG	This paper	N/A
Deposited Data		
Raw Western Blot and Microscopy Data	Mendeley	https://doi.org/10.17632/8t7xh2ck55.1
RNAseq data	GEO	GSE210129
Mass Spectometry data	PRIDE	PXD035353
Software and algorithms		
Affinity Designer	Affinity	https://affinity.serif.com/en-gb/designer/
Affinity Photo	Affinity	https://affinity.serif.com/en-gb/photo/
Benchling	https://www.benchling.com	N/A
Fiji (ImageJ)	NIH	https://imagej.nih.gov/ij/docs/guide/146-2.html
GraphPad Prism 9	GraphPad	https://www.graphpad.com/scientific-software/prism/
ScanR acquisition software	Olympus	https://www.olympus-lifescience.com/en/microscopes/inverted/scanr/#!
ScanR analysis software	Olympus	https://www.olympus-lifescience.com/en/microscopes/inverted/scanr/#!
TIBCO Spotfire	Perkin Elmer	https://www.perkinelmer.com/product/tibco-spotfire-in-research-spotfirer
Other		
96-well microplates (CELL CULTURE MICROPLATE, 96 WELL, PS, F-BOTTOM (8 × 4, 32 stk/pack))	Greiner-BIO	Cat# GR-655090
Corning® 96-well Flat Clear Bottom Black Polystyrene TC-treated Microplates	Corning	Cat# 3904
DharmaFECT™ siRNA transfection reagents	VWR	Cat# T-2001-03
Phosphatase inhibitor tablets (PhosSTOP; cOmplete ULTRA Tablets, Mini, EASYpack)	Roche	Cat# 000000004906837001
Protease inhibitor tablets (cOmplete ULTRA Tablets, Mini, EASYpack Protease Inhibitor Cocktail)	Roche	Cat# 000000005892970001
PureProteome Protein G Magnetic Bead System	Sigma-Aldrich	Cat# LSKMAGG02

(*Continued on next page*)

Continued

REAGENT or RESOURCE	SOURCE	IDENTIFIER
QuikChange II Site-Directed Mutagenesis Kit	Agilent	Cat# 200523
BamHI, EcoRI, HpaI, rCutsmart	New England Biolabs	Cat# R0136S, R3101S, R0105S, B6004S

RESOURCE AVAILABILITY

Lead contact

Further information and requests for resources and reagents should be directed to and will be fulfilled by the lead contact, Luis Ignacio Toledo (ltoledo@sund.ku.dk).

Materials availability

All unique reagents generated in this study are available from the lead contact upon request.

Data and code availability

- Original Western data and microscopy data for figures in this paper have been deposited at Mendeley Data and are publicly available as of the date of publication. The DOI is listed in the key resources table. RNA-seq and Mass Spectrometry data have been deposited at GEO and PRIDE (ProteomeXchange Consortium) (Perez-Riverol et al., 2022), respectively, and are publicly available as of the date of publication. Accession numbers are listed in the key resources table.
- This paper does not report original code.
- Any additional information required to reanalyze the data reported in this paper is available from the lead contact upon request.

EXPERIMENTAL MODEL AND SUBJECT DETAILS

Cell culture

All cell lines used in this study were grown at 37°C and 5% CO_2 in Dulbecco's modified Eagle's medium (DMEM, high glucose, GlutaMAX), supplemented with 6% fetal bovine serum (FBS) and Penicillin-Streptomycin (10,000 U/mL) all from Thermo Fisher Scientific. Cells were monthly verified to be free of mycoplasma contamination.

Cell lines

U2OS and hTERT-RPE1 cells were obtained from ATCC. HeLa and MCF7 cells were provided by Ian Hickson (Center for Chromosomal Stability, University of Copenhagen). HeLa cells stably expressing CDK2L-GFP were a kind gift from Alexis Barr (MRC, London Institute of Medical Sciences, Imperial College). U2OS cells harboring a doxycycline-inducible TRESLIN WT or TASA construct were a kind gift from Christopher Sansam (Department of Cell Biology, University of Oklahoma). U2OS cells stably expressing AcGFP-TRESLIN WT or TASA construct were published previously (Boos et al., 2013; Ferreira et al., 2022). U2OS cells with endogenously GFP-tagged CDC45 were a kind gift from Jiri Lukas (Novo Nordisk Foundation Center for Protein Research, University of Copenhagen). Stable MTBP transgene–expressing HeLa Flip-In T-Rex cell lines (Fahrenkamp et al., 2015) were generated according to the manufacturer's instructions (Invitrogen) using pcDNA5-FRT-TO-Flag3-Tev2-GFP or pcDNA5-FRT-TO-Flag3-Tev2. HeLa cells stably expressing mTurquoise2–$SLBP_{18-126}$ (kind gift from Michael Lin, Addgene #83842, (Bajar et al., 2016)) were generated by lentiviral infection. U2OS cells stably expressing AcGFP-TRESLIN WT and CDC45-3xFLAG were generated by lentiviral infection with FUW-CDC45-3xFLAG construct.

METHOD DETAILS

Cloning of FUW-CDC45-3xFLAG

To generate FUW-3xFLAG, FUW (Addgene #14882) was digested using restriction enzymes HpaI and EcoRI and ligated with 3xFLAG oligos (annealed and digested with HpaI and EcoRI):

Forward: 5'GTCCTGGTTAACGACTACAAAGACCATGACGGTGATTATAAAGATCATGACATCGACTACAAGGATGACGATGACAAGTAGGAATTCGTCCTG 3'

Reverse:

5'CAGGACGAATTCCTACTTGTCATCGTCATCCTTGTAGTCGATGTCATGATCTTTATAATCACCGTCATGGTCTTTGTAGTCGTTAACCAGGAC 3'.

Generation of siRNA resistant CDC45 was achieved according to the manufacturer's instructions (Agilent) using:

Forward primer: 5' CGTCAATGTATACAACGACACGCAAATCAAATTACTCATTAAAC 3' and reverse primer: 5' GTTTAATGAGTAATTTGATTTGCGTGTCGTTGTATACATTGACG 3'.

CDC45 was amplified by PCR using:

Forward primer (BamHI overhang): 5' CGAAGCGGATCCATGTTCGTATCCGATTTCCG 3' and reverse primer (HpaI overhang): 5' CGAAGCGTTAACGGACAGGAGGGAAATAAGTG 3'.

To generate FUW-CDC45-3xFLAG, FUW-3xFLAG was digested using restriction enzymes HpaI and BamHI and ligated with CDC45 (digested with HpaI and BamHI). Mutagenesis and plasmids were confirmed by sequencing.

Drugs and cell culture supplements

Hydroxyurea (Sigma-Aldrich), ATRi (AZ20, Selleckchem), CHK1i (AZD7762, Selleckchem), WEE1i (MK1775, Selleckchem), PLK1i (B2536, Selleckchem), CDK2i II (Calbiochem), AURORA Ai (MLN8237, Selleckchem) and CDC7i (XL413, AdooQ Bioscience) were used as indicated in the corresponding figure legends. Doxycycline (Sigma-Aldrich) was used at 1μg/mL for 24 hours to induce expression of the plasmid integrated in the cell line. dNTP analogs Thymidine (Sigma-Aldrich), BrdU (Sigma-Aldrich) and EdU (Sigma-Aldrich) were used where indicated. DMSO (Sigma-Aldrich) was used, where indicated, at the same concentration as the drug used in parallel.

Gene silencing by siRNA

Transfection of siRNA duplexes were performed using DharmaFECT™ (VWR) following manufacturer's guidelines. All siRNAs were used at 10nM, unless specified otherwise. Transfections were performed for either 48 or 72 hours (specified in figure legends). A 1:1 mix of MTBP #1 and #2; of ETAA1 #3 and #4; TIMELESS #1 and #2 was used.

Immunostaining

Cells were grown in 96-well mircoplates (Greiner-BIO) before being fixed in formaldehyde 4% (VWR) at room temperature (RT) for 10 minutes (min). To study chromatin bound proteins, cells were pre-extracted, prior fixation, using 0.5% Triton X-100 in PBS on ice for 1 min. After fixation, cells were permeabilized using 0.5% Triton X-100 in PBS at RT for 20 min. Permeabilization step was skipped for pre-extracted cells. Primary antibodies were diluted in filtered DMEM containing 6% FBS. Cells were stained at RT for 1 hour, followed by 3 washes with 0.01% PBS-Tween 20. For EdU detection, cells were incubated with Click iT buffer (100 mM Tris-HCl pH 8, 2 mM CuSO4, 1 ng Alexa Fluor 647 Azide (Jena Bioscience) and 100mM ascorbic acid) at RT for 1 hour, followed by 3 washes with 0.01% PBS-Tween 20. Secondary antibodies and DAPI were diluted in filtered DMEM containing 6% FBS. Cells were stained at RT for 1 hour. After 3 final washes with 0.01% PBS-Tween 20, cells were stored in PBS at 4°C until imaging.

Microscopy and Quantitative Image Based Cytometry (QIBC)

Images used for QIBC were obtained with the ScanR acquisition software controlling a motorized Olympus IX-83 wide-field microscope. The system was equipped with filter cubes compatible with DAPI, FITC, Cy3, and Cy5 fluorescent dyes, a Spectra X-LIGHT engine Illumination system with 6 color LEDs and emission filters and a Hamamatsu Camera Orca Flash 4.0 V2. Olympus Universal Plan Super Apo 10x Objective was used for all QIBC data presented in this study. Using the ScanR image analysis software, images were processed and TIBCO Spotfire® software was used to plot total nuclear pixel intensities (Arbitrary units: A.U.) and mean (total pixel intensities divided by nuclear area) nuclear intensities (A.U.) for DAPI and all other parameters (each of them specified in the corresponding figure legend) in color-coded scatter diagrams. DNA content is plotted on the x-axis using total DAPI intensities in linear scale. Parameters plotted on the y-axis are mean intensities in logarithmic scale (only CDK1/2 activity is in linear scale). In all scatter plots 2000 random cells are visualized. TIBCO Spotfire® software was used to analyze the percentages of mitotic cells based on H3-pS10 staining. Different cell cycle populations were gated using EdU and DAPI stainings. Averages of mean intensities were analyzed within these subpopulations. Images of Figures 1A, 1F, 2D, 2I, and S1I (alpha-tubulin), Figures S2F and S2G were taken on the same Olympus IX83-ScanR system using an Olympus Plan Semi Apo 40x objective (UPLXAPO40X). Images of Figure 2I (H3-pS10 and RPA32), Figures 6D and 7C were taken on the same Olympus IX83-ScanR system using an Olympus 60X silicone immersion objective (UPLSAPO60XS). Images of Figure S2B were taken on the same Olympus IX83-ScanR system using an Olympus Plan Semi Apo 20x objective (UPLXAPO20x). Images of Figure 3G were taken on the same Olympus IX83-ScanR system using an Olympus Plan Apo 10x objective (UPLXAPO10X). Representative images were analyzed using the Fiji (ImageJ) software. Images of Figure 6G were taken on a Zeiss LSM 800 confocal microscope using a 40x objective (Zeiss Plan-Apochromat 40x/1.3 Oil DIC).

Color gradients and thresholds used in QIBC scatter plots are meant to visually enhance the differences in intensities among the experimental conditions. For cell cycle markers such as CyclinB and H3-pS10, thresholds were chosen according to cell cycle transitions in control conditions, highlighting the different intensities within G2 vs G1-S or M. For CB-TRESLIN-GFP (Figure 6), thresholds highlight the intensities in G1 vs S/G2 in control conditions. For γH2AX (Figures 3 and 5) thresholds highlight the intensity above the majority of cells (>90%) in untreated conditions.

Chromatin and soluble fractionations

Cells were seeded in 10cm dishes and treated as indicated in the corresponding figure legends. Cells were washed with ice-cold PBS and harvested by trypsinization. Cells were incubated with ice-cold 0.5% Triton X-100 in PBS supplemented with protease and phosphatase inhibitors (Roche) on ice for 30 min. Fractions were centrifuged at 17000 g at 4°C for 10 min. Supernatant was collected for the soluble proteins and the remaining pellet was incubated again with 0.5% Triton X-100 in PBS supplemented with protease and

phosphatase inhibitors (Roche) on ice for 30 min. Fractions were centrifuged at 17000 g at 4°C for 10 min. Supernatant was discarded and the remaining pellet was dissolved in RIPA (50 mM Tris-HCl pH 8, 150 mM NaCl, 1% IGEPAL CA-630, 0.1% SDS, 0.1% Na-deoxycholic acid) supplemented with protease and phosphatase inhibitors (Roche) and Benzonase® Nuclease (Sigma-Aldrich) for 30 min on ice and clarified by centrifugation at 17000 g at 4°C for 10 min. Supernatant was collected in a new tube and processed for immunoblotting, pellet was discarded.

Immunoprecipitation

Cells were seeded in 15cm dishes and treated with control or TRESLIN siRNA for 48 hours. Cells were washed with ice-cold PBS and harvested by trypsinization. Cells were lysed in lysis buffer (50 mM Tris-HCl pH 7.7, 150 mM NaCl, 0.5% NP40) supplemented with protease and phosphatase inhibitors (Roche) on ice and clarified by centrifugation at 17000 g at 4°C for 10 min. Supernatant was collected in a new tube and pellet was discarded. PureProteome Protein G Magnetic Beads were prepared following manufacturer's instructions (Sigma-Aldrich). In brief, magnetic beads were washed with PBS containing 0.1% Tween 20 before 2 μg of the capture antibody (CDK1 or CDK2) was added. Capture antibodies and beads were incubated at RT for 10 min using continuous mixing. Beads were washed 3 times with PBS 0.1% Tween 20, before beads were incubated overnight with the sample (siCTR or siTRESLIN) at 4°C with continuous mixing. Beads were washed 3 times with PBS containing 0.1% Tween 20. Beads were resuspended in Laemmli sample buffer (120mM Tris-Cl pH 6.8, 4% SDS, 20% glycerol) and processed for immunoblotting.

Immunoblotting

To collect whole cell extracts (WCE), cells were seeded in 10cm dishes and treated as indicated in the corresponding figure legends. Cells were washed with ice-cold PBS and harvested by trypsinization. Cells were lysed in RIPA (50 mM Tris-HCl pH 8, 150 mM NaCl, 1% IGEPAL CA-630, 0.1% SDS, 0.1% Na-deoxycholic acid) supplemented with protease and phosphatase inhibitors (Roche) and Benzonase® Nuclease (Sigma-Aldrich) for 30 min on ice and clarified by centrifugation at 17000 g at 4°C for 10 min. Supernatant was collected in a new tube and pellet was discarded. 4x LDS Loading Dye (Sigma-Aldrich) and 1,4-Dithiothreitol (DTT; Sigma-Aldrich) were added to immunoprecipitation samples, WCE and chromatin fractions. Samples were boiled at 95°C for 5 min. For immunoprecipitation samples, beads were removed before samples were analyzed by SDS-PAGE.

Primary antibodies were incubated overnight at 4°C in 0.05% PBS-Tween 20 containing 5% milk. For phospho antibodies, milk was replaced by bovine serum albumin (BSA). Treslin antibody was diluted in 0.05% PBS-Tween 20 containing 1% milk. Secondary peroxidase-coupled antibodies were diluted in 0.05% PBS-Tween 20 containing 5% milk and incubated for 1 hour at RT. ECL-based chemiluminescence was detected using an Amersham Imager 600.

Mass Spectrometry - whole proteome sample preparation

Snap-frozen HeLa cell pellets were lysed in 20% [v/v] 2,2,2-trifluoroethanol in 100 mM Tris-HCl, pH 8.0 supplemented with 5 mM DTT and heated for 10 min at 95 °C. Lysates were sonicated in a Biorupter (Diagenode) for 15 min prior to addition of 25 mM chloroacetamide and incubated for 20 min. Samples were eluted in 100 mM Tris-HCl, pH 8.0 and digested with trypsin (1:50) overnight at 37 °C at 1500 rpm. Peptides were desalted and purified with styrene divinylbenzene-reversed phase sulfonate (SDB-RPS) StageTips prepared in 0.2% trifluoroacetic acid (TFA). Peptides were washed and eluted with 80% acetonitrile (ACN); 1% ammonia prior to vacuum-drying. Dried peptides were reconstituted in 2% ACN and 0.1% TFA. For deep proteome coverage, peptide samples from siTreslin (48h) and siCtrl HeLa cells were further fractionated into eight fractions by high pH reversed-phase fractionation as previously described (Kulak et al., 2017).

Mass Spectrometry - LC-MS analysis

Nanoflow LC–MS/MS analysis of tryptic peptides was conducted on a quadrupole Orbitrap mass spectrometer (Q Exactive HF-X, ThermoFisher Scientific, Bremen, Germany) (Kelstrup et al., 2018) coupled to an EASY nLC 1200 ultra-high-pressure system (Thermo Fisher Scientific) via a nano-electrospray ion source. Three hundred ng of peptides were loaded on a 50-cm HPLC-column (75 μm inner diameter, New Objective, Woburn, MA, USA; in-house packed using ReproSil-Pur C18-AQ 1.9-μm silica beads; Dr Maisch GmbH, Ammerbuch, Germany). Peptides were separated using a linear gradient from 2 to 20% B in 55 min and stepped up to 40% in 40 min followed by a 5 min wash at 98% B at 350 nl per min where solvent A was 0.1% formic acid in water and solvent B was 80% ACN and 0.1% formic acid in water. The total duration of the run was 100 min. Column temperature was kept at 60 °C using an in-house-developed oven. The mass spectrometer was operated in 'top 15' data dependent mode, collecting MS spectra in the Orbitrap mass analyzer (60,000 resolution, 300–1,650 m/z range) with an automatic gain control (AGC) target of 3E6 and a maximum ion injection time of 25 ms. The most intense ions from the full scan were isolated with an isolation width of 1.4 m/z. Following higher energy collisional dissociation (HCD) with a normalized collision energy (NCE) of 27, MS/MS spectra were collected in the Orbitrap (15,000 resolution) with an AGC target of 1E5 and a maximum ion injection time of 28 ms. Precursor dynamic exclusion was enabled with a duration of 30 s.

Mass Spectrometry data analysis

Raw files were processed with MaxQuant (Cox and Mann, 2008) (version 1.6.5.0). The integrated Andromeda search engine (Cox et al., 2011) was used for peptide and protein identification at an FDR of less than 1%. The human UniProtKB database (October

2019) was used as forward database and the automatically generated reverse database for the decoy search. 'Trypsin' was set as the enzyme specificity. Search criteria included carbamidomethylation of cysteine as a fixed modification and oxidation of methionine and acetyl (protein N-terminus) as variable modifications. A minimum of 7 amino acids were required for peptide identification. Proteins that could not be discriminated by unique peptides were assigned to the same protein group. Label-free protein quantification was performed using the MaxLFQ (Cox et al., 2014) algorithm and 'match-between-runs' was enabled. Proteins, which were found as reverse hits or only identified by site-modification, were filtered out prior to data analysis.

RNAseq library preparation and sequencing

Total RNA was extracted from cells using manufacturer's instructions (Cytiva Life Sciences). mRNA with polyA tail was enriched using oligo dT beads, fragmented and reversed transcribed to cDNA by N6 random primer. cDNA was repaired with phosphate at 5' end and stickiness "A" at 3' end, followed by ligation of an adaptor with stickiness "T" at 3' end to the cDNA. Ligation product was amplified by PCR. PCR was denatured by heat and ssDNA was cyclized by splint oligo and DNA ligase. Samples were analyzed using BGISEQ-500 sequencer and trimming was done by adaptor removal and low quality reads removal.

RNA-seq data processing and analysis

The quality of the sequenced reads was assessed using FastQC (v. 0.10.1; https://www.bioinformatics.babraham.ac.uk/projects/fastqc/), FastqScreen (v. 0.11.4; PMID: 30254741), and MultiQC (v. 1.7; PMID: 27312411). Reads were trimmed by BGI prior to release and mapped to canonical chromosomes from hg38 using STAR (v. 2.5.1a; PMID: 23104886) using the setting "–outFilterMismatchNoverLmax 0.1 –outFilterMatchNmin 16 –outFilterMismatchNmax 5. Transcriptome annotation was retrieved from Refseq (PMID: 26553804) on 2018-08-05 and fed into HTseq-count to quantify reads within transcripts using the settings 'htseq-count –mode=union –stranded=no'. Output was converted to bam files using Samtools (v. 1.10)(PMID: 19505943. Differential expression analysis was done using R (v.4.0.2; COMMENT: Guide to citation here: https://www.r-bloggers.com/2018/06/its-easy-to-cite-and-reference-r/) and DeSeq2 (PMID: 25516281). RNA-seq and proteome data were integrated based on gene Gene symbols, and the subsets of genes, which had significantly different expression in the RNA-seq data at 24 or 48 hours (adjusted p-values of 0.05 or lower), were compared based on the $\log_2$ fold differences in the proteome data using R and a two-sided Fischer's exact test.

QUANTIFICATION AND STATISTICAL ANALYSIS

Statistical analysis was performed in Graphpad Prism 9 using unpaired t-tests. Statistical details can be found in the corresponding figure legend, as well as the number of cells analyzed and number of replicates.